

Electronic version of an article published as Journal of Porphyrins and Phthalocyanines 25, No. 07, 2021, 639-663 <https://doi.org/10.1142/S1088424621500620> © [copyright World Scientific Publishing Company] <https://www.worldscientific.com/doi/pdf/10.1142/S1088424621500620>

Citation:

Kang, Hyun Suk et al. Conjugated-linker dependence of the photophysical properties and electronic structure of chlorin dyads. Journal of Porphyrins and Phthalocyanines 25, No. 07 (2021): 639-663. <https://www.worldscientific.com/doi/10.1142/S1088424621500620>

DOI:

<https://doi.org/10.1142/S1088424621500620>

Access to this work was provided by the University of Maryland, Baltimore County (UMBC) ScholarWorks@UMBC digital repository on the Maryland Shared Open Access (MD-SOAR) platform.

Please provide feedback

Please support the ScholarWorks@UMBC repository by emailing scholarworks-group@umbc.edu and telling us what having access to this work means to you and why it's important to you. Thank you.

**Conjugated-Linker Dependence of the Photophysical Properties and
Electronic Structure of Chlorin Dyads**

Hyun Suk Kang,[†] Andrius Satraitis,[‡] Adam Meares,[‡] Ganga Viswanathan Bhagavathy,[‡]

James R. Diers,[§] Dariusz M. Niedzwiedzki,[#] Christine Kirmaier,[†]

Marcin Ptaszek,^{*,‡} David F. Bocian,^{*,§} and Dewey Holten^{*,†}

[†]Department of Chemistry
Washington University
St. Louis, Missouri 63130-4889, United States

[‡]Department of Chemistry and Biochemistry
University of Maryland, Baltimore County
Baltimore, Maryland 21250, United States

[§]Department of Chemistry
University of California
Riverside, California 92521-0403, United States

[#]Center for Solar Energy and Energy Storage, and
Department of Energy, Environmental & Chemical Engineering
Washington University
St. Louis, MO 63130-4889
United States

ABSTRACT

The synthesis, photophysical properties and electronic structure of seven new chlorin dyads and associated benchmark monomers are described. Each dyad contains two identical chlorins linked at the macrocycle β -pyrrole 13-position. The extent of electronic communication between chlorin constituents depends on the nature of the conjugated linker. The communication is assessed by modification of prominent ground-state absorption and redox properties, rate constants and yields of excited-state decay processes, and molecular-orbital characteristics. Relative to the benchmark monomers, the chlorin dyads in toluene exhibit a substantial bathochromic shift of the long-wavelength absorption band (30 nm average), two-fold increased radiative rate constant [average $(10\text{ ns})^{-1}$ vs $(22\text{ ns})^{-1}$], reduced singlet excited-state lifetimes (average 5.0 ns vs 8.2 ns), and increased fluorescence quantum yields (average 0.56 vs 0.42). The excited-state lifetime and fluorescence yield for the chlorin dyad with a benzothiadiazole linker are reduced substantially in benzonitrile versus toluene due largely to ~ 25 -fold accelerated internal conversion. The results aid design strategies for molecular architectures that may find utility in solar-energy conversion and photomedicine.

I. INTRODUCTION

The design of chromophores with strong absorption in the far red and near-infrared (NIR) spectral region has been motivated in part by potential utility in solar-energy conversion and photo-medical research. Light-harvesting systems with such characteristics are of interest because over half of the solar radiation reaching the earth is in the NIR [1]. Biomedical applications such as photodynamic therapy, optical imaging, and photoacoustic spectroscopy are aided by pigments that have strong NIR absorption because of the comparatively low background absorption by endogenous species *in vivo* [2,3]. Of the three key tetrapyrrole families, the long-wavelength absorption band is typically in the green-orange region for porphyrins, in the red region for chlorins, and in the NIR for bacteriochlorins [4–6]. For example, the natural photosynthetic pigments chlorophyll *a* and bacteriochlorophyll *a* in organic solvents typically absorb at roughly 665 and 775 nm, respectively [7]. The use of substituents on the macrocycle and fused annulated rings have been utilized to shift the long-wavelength absorption band of chlorins and bacteriochlorins to progressively longer wavelengths [8–12].

Strong linker-mediated electronic coupling between tetrapyrroles has been employed as another means of shifting the absorption spectra of members of all three tetrapyrrole families deeper into the red and NIR regions [13]. This strategy was pioneered for porphyrins [14–29] and extended more recently to the construction of chlorin-chlorin [30–34], bacteriochlorin-bacteriochlorin [35] and chlorin-bacteriochlorin [36,37] dyads. Bathochromic shifts in the long-wavelength ($S_0 \rightarrow S_1$) absorption are underpinned by linker-mediated mixing of the frontier molecular orbitals (MOs). The mixing engenders a reduction in the energy gap between the highest filled MO (HOMO) and lowest unoccupied MO (LUMO). The HOMO \rightarrow LUMO electron promotion makes an important contribution, along with electron promotions involving

the HOMO-1 and LUMO+1, to the optical spectra of tetrapyrroles, including the wavelength and intensity of the lowest energy (longest wavelength) absorption band within Gouterman's four-orbital model [4–6].

In previous studies, we explored the relationship between chemical structure and photophysical properties of sets of chlorin and bacteriochlorin dyads [35,38]. The electronic communication within each dyad is mediated by either an ethynyl or butadiynyl bridge at the macrocycle β -pyrrole (13-) or *meso*-bridge (15-) positions. These two-types of chlorin-chlorin dyads are shown in Chart 1. The effects of strong coupling between the two constituents of each dyad are manifested by altered ground-state properties including splitting in the redox waves for the first oxidation and first reduction. The effects of strong coupling are also manifested in the excited state via mixing of one-electron configurations arising from electron promotions involving the pairs of "HOMOs", "LUMOs", "HOMO-1" and "LUMO+1." In particular, the absorption spectra show splitting and shifting of nominally similar features in the dyad compared to those of the monomer, including an intensification of the long-wavelength band. Photophysical properties of the lowest singlet-excited state (S_1) such as the lifetime, and the yields and rate constants for the $S_1 \rightarrow S_0$ fluorescence, $S_1 \rightarrow T_1$ intersystem crossing, and $S_1 \rightarrow S_0$ internal conversion pathways also differ for the dyads versus the constituents [38].

There have been systematic studies of the optical spectra of porphyrin dyads as a function of linker type [21,23]. On the other hand, the effects of the nature of the linker have not been explored extensively for chlorin or bacteriochlorin dyads. The present paper extends our prior studies to examination of the photophysical, redox, and MO properties of a series of dyads in which two identical chlorins are joined at the β -pyrrole (13-) position by a various conjugated linkers including butadiyne, ethyne, vinyl, and others that possess an aromatic unit sandwiched between two ethynes (Chart 2). The properties of the dyads are examined using electrochemistry,

static and time-resolved optical studies, and density functional theory (DFT) calculations. These results should aid the design of tetrapyrrole dyads that exhibit strong absorption in the far red and NIR regions along with favorable excited-state properties.

Chart 1. Molecular Structures of Chlorin Dyads and Benchmarks Studied Previously.

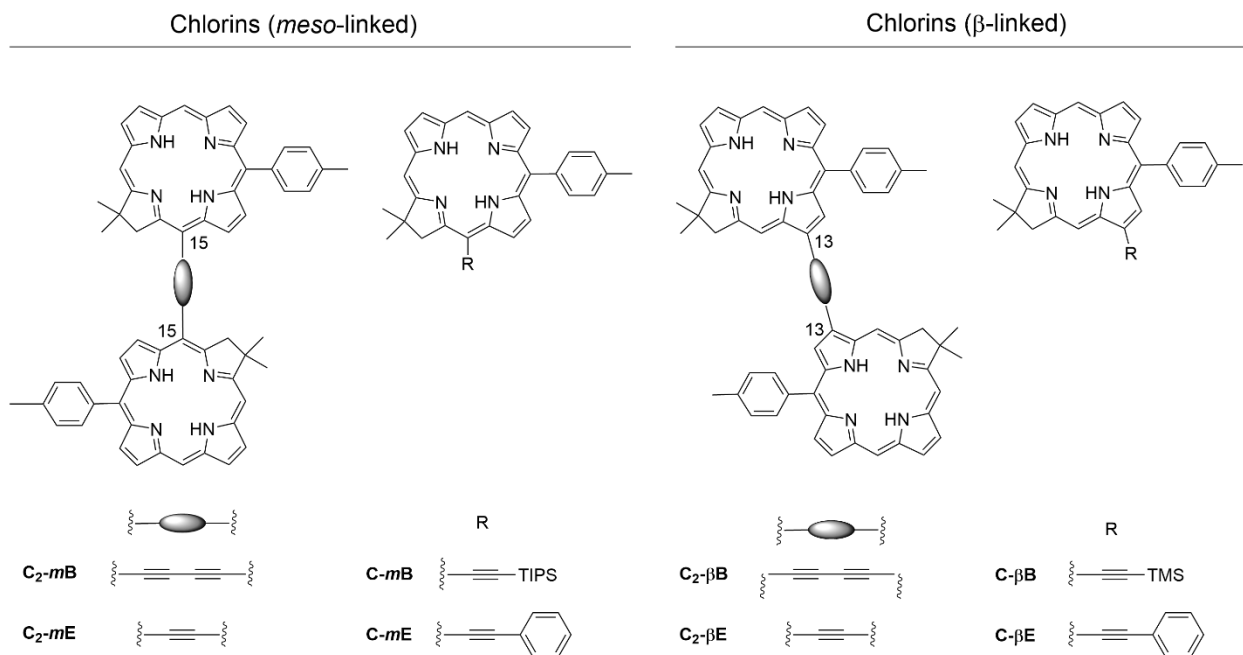
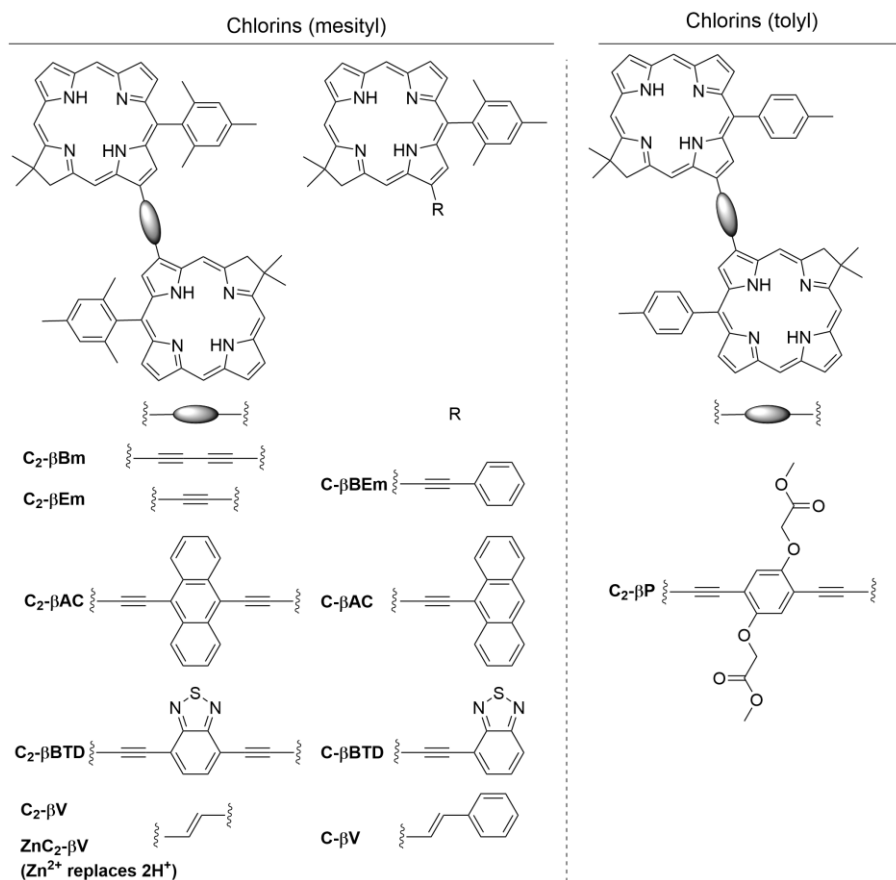


Chart 2. Molecular Structures of Chlorin Dyads and Benchmarks Studied Here.



II. EXPERIMENTAL SECTION

A. Synthetic Compounds. The dyads **C₂-βB** [35], **C₂-βE** [35], **C₂-βEm** [39], **C₂-βV** [39], **ZnC₂-βV** [39], and monomers **C-βE** [35], **C-βB** [35], **C-βEm** [40], and **C-βV** [39] were synthesized previously. The details of synthesis of all new dyads and monomers are reported in the *Supporting Information*.

B. Photophysical Properties. Photophysical measurements were performed on dilute (μM) solutions in toluene or benzonitrile at room temperature. Static absorption spectra were acquired using a Shimadzu UV-1800 spectrometer and static emission studies utilized a Horiba

Nanolog spectrofluorometer. Samples were Ar-purged for determination of the singlet excited-state (S_1) lifetime (τ_S), $S_1 \rightarrow S_0$ fluorescence quantum yield (Φ_f), and yield of intersystem crossing (Φ_{isc}) from S_1 to the lowest triplet excited state (T_1), i.e., the triplet yield. The Φ_f measurements used samples with absorbance ≤ 0.1 at the 500–550 nm excitation wavelength. The reported Φ_f value for each compound is the average from two methods: (1) relative to and *meso*-tetraphenylporphyrin in non-degassed toluene ($\Phi_f = 0.070$ [11]) as the standard and (2) using an integrating sphere (Horiba Quanti-Phi). Transient absorption studies (e.g., to obtain τ_S and Φ_{isc}) employed attenuated (0.5–1 μ J) ~ 100 fs excitation flashes (typically at the long-wavelength absorption maximum) from a 1 kHz Ti:sapphire laser system with optical parametric amplifier (Spectra Physics). Measurements employed two transient-absorption setups (Ultrafast Systems). One instrument (Helios) with ~ 100 fs white-light probe pulses and an optical pump-probe delay up to ~ 8 ns was used for samples with $\tau_S \leq 1$ ns. A second spectrometer (EOS) with ~ 1 ns probe pulses and detection in 0.1 ns bins for times to 0.5 ms was additionally used for samples with $\tau_S > 1$ ns. The Φ_{isc} values were obtained by comparing the extent of ground-state bleaching due to S_1 at early times to that for T_1 at the asymptote of the S_1 decay, both referenced to the flanking relatively featureless excited-state absorption.

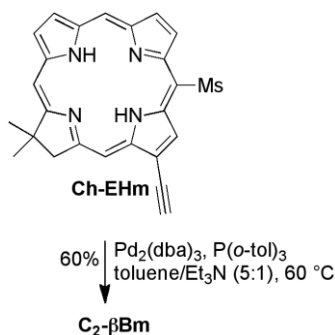
C. Electrochemistry. Electrochemical studies were performed using a standard three-electrode cell, as described previously [41].

D. Computational Calculations. DFT calculations were performed on all the dyads with Spartan'10 for Windows (Wavefunction Inc. Irvine, CA) using the B3LYP functional and 6-31G* basis set in vacuum [42]. Full structure geometry optimization was performed for each run. For the dyads, several geometries with different torsional angles (about the linker) between the macrocycles were examined to locate the conformation corresponding to the global energy

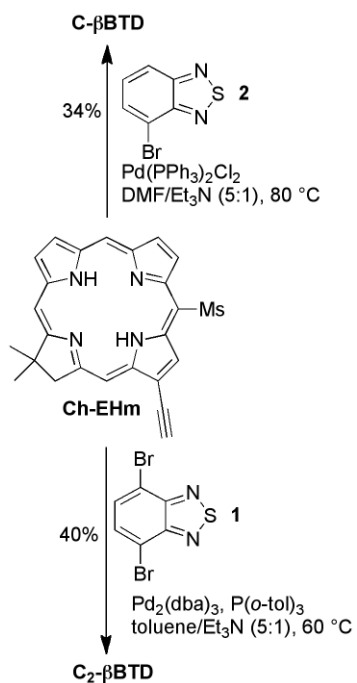
minimum. The energies for conformations with different torsional angles between the macrocycles were computed by fixing the torsional angle at a specified value, followed by optimizing the geometry of the rest of the structure.

III. RESULTS

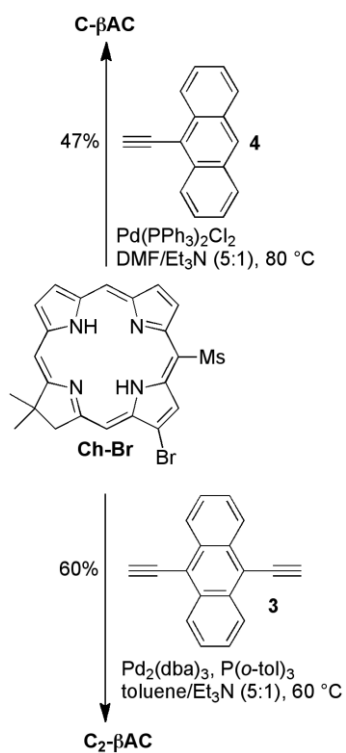
A. Synthesis. The new dyads reported here were synthesized following the general strategy outlined previously [35]. The butadiyne-linked **C₂-βBm** was synthesized by a palladium-catalyzed homocoupling of ethynyl-substituted chlorin **Ch-EHm** [39] in 63% yield (Scheme 1). Dyad **C₂-βBTD** was synthesized in 40% yield through reaction of **Ch-EHm** with dibromide **1** (Scheme 2). A significant amount of homocoupled product **C₂-βBm** was also produced in this reaction. Corresponding benchmark monomer **C-βTBD** was synthesized in Sonogashira reaction of **Ch-EHm** with commercially available monobrominated compound **2** in 34% yield (Scheme 2). **C₂-βAC** was obtained from reaction of bromochlorin **Ch-Br** [43] with 9,10-diethynylantracene **3** [44] in 60% yield, while monomer **C-βAC** was obtained in reaction of the same **Ch-Br** with 9-ethynylantracene **4** [45], in 47% yield (Scheme 3). Dyad **C₂-βP** was prepared in a Sonogashira reaction of **Ch-EH** [27] with dibromide **5** in 25% yield (Scheme 4). All new dyads and monomers were characterized by ¹H NMR and HRMS, most of them by ¹³C NMR. The data are consistent with the expected structures.



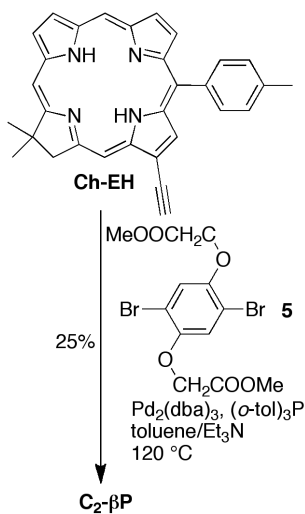
Scheme 1. Synthesis of dyad **C₂-βBm**.



Scheme 2. Synthesis of dyad **C₂-βBTD** and corresponding benchmark monomer **C₂-βBTD**.



Scheme 3. Synthesis of dyad **C₂-βAC** and corresponding benchmark monomer **C₂-βAC**.



Scheme 4. Synthesis of dyad **C₂-βP**.

B. Electronic Ground-State Absorption Spectra. The electronic ground-state absorption spectra of the chlorin dyads in toluene are shown in Figure 1. Similar spectra are observed in benzonitrile (Figure S1). The optical characteristics are summarized in Tables 1 and S1.

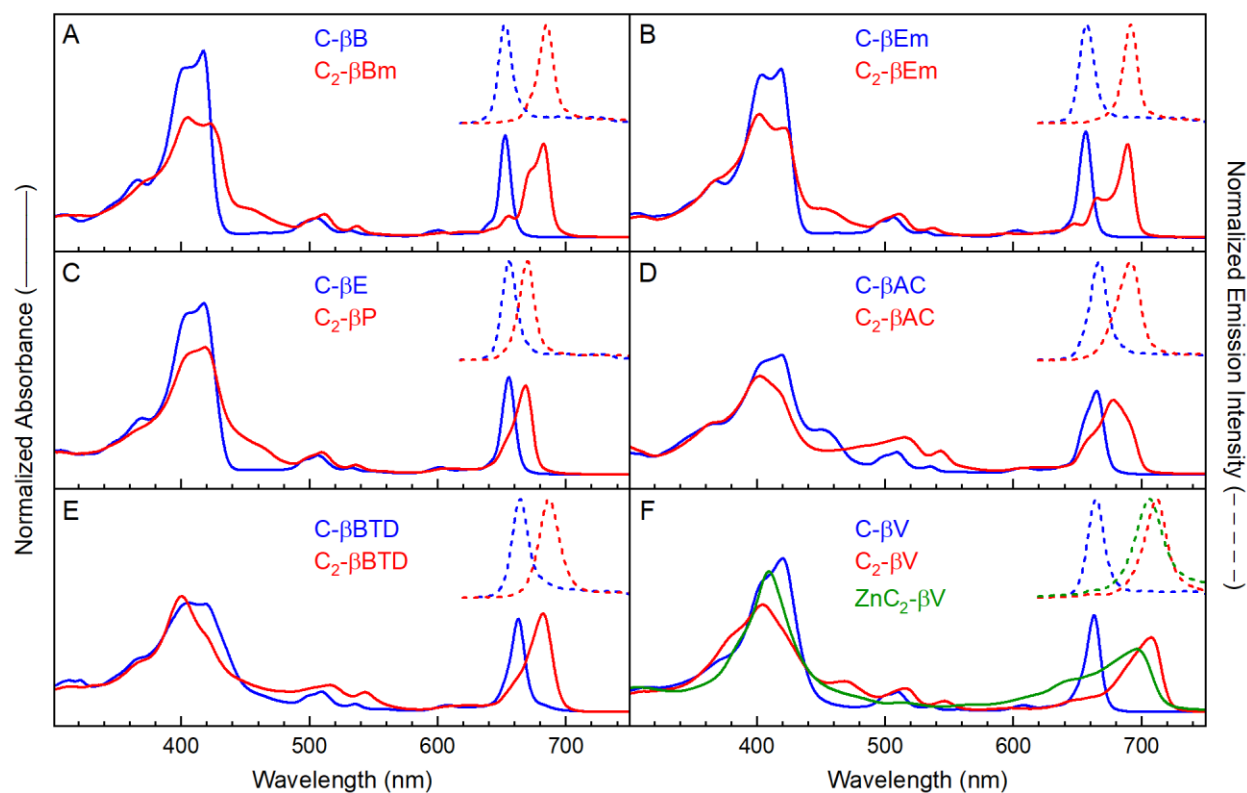


Figure 1. Absorption (solid) and fluorescence emission spectra (dashed) of the chlorin dyads (red) and benchmarks (blue) in toluene. Absorption spectra were normalized to the total integrated intensity (300–900 nm for spectra plotted vs cm^{-1}), and all fluorescence spectra (500–550 excitation) were normalized to the peak intensity.

Table 1. Spectral Characteristics of Chlorin Dyads and Benchmarks in Toluene.

Compound	λ_B (nm)	λ_{Q2} (nm)	$\Delta\lambda_{Q2}^{\text{shift}}$ (cm ⁻¹)	$\lambda_{Q1\beta}$ (nm)	$\lambda_{Q1\alpha}$ (nm)	$\Delta\lambda_{Q1}^{\text{shift}}$ (cm ⁻¹)	$\Delta\lambda_{Q1}^{\text{split}}$ (cm ⁻¹)	λ_{em} (nm)	fwhm em (nm)
<i>Current Dyads</i>									
C₂-βBm	403, 426, 452	537	175	672	683	460	240	685	13
C₂-βEm	401, 424, 452	537	175	665	690	456	545	692	12
C₂-βP	404, 421, 445	536	140	662 ^a	670	205	180	670	14
C₂-βAC	401, 458 ^a	543	275	678	691 ^a	427	277	691	21
C₂-βBTD	400, 420, 442 ^a	543	275	665 ^a	682	233	375	687	18
C₂-βV	381, 404, 470	547	375	697 ^a	710	867	263	712	21
ZnC₂-βV	409	513		665 ^a	696		670	706	26
<i>Prior Dyads</i>									
C₂-βB	404, 422, 452	538	210	672	681	555	197	681	13
C₂-βE	402, 417, 452	538	174	664	687	436	504	687	13
<i>Current Benchmark Monomers</i>									
C-βEm	404, 419	532			657			658	14
C-βAC	419, 450	535			665			666	16
C-βBTD	420, 460	535			663			665	14
C-βV	405, 420	536			663			665	14
<i>Prior Benchmark Monomers</i>									
C-βB	401, 417	532			652			652	13
C-βE	403, 418	533			656			656	13

^aShoulder on the main feature.

The absorption spectra of the benchmark chlorins show the typical set of origin transitions: intense near-ultraviolet Soret (B_x and B_y) bands, a weak Q_x band in the green-yellow region, and a moderately strong red-NIR Q_y band. The Q_x and Q_y manifolds each contain one or more vibronic satellite features built on the origin band with a spacing of 1000–1400 cm^{-1} . The B_y band is typically at shorter wavelength than the B_x band for chlorins. For the chlorin monomers studied here, the B_y and B_x origin bands have maxima in range of 401–420 nm and 417–460 nm, respectively, but are substantially overlapped (Figure 1 and Table 1). Features that could represent vibronic satellites built on the B_y and B_x origin bands are seen in some cases, although such features could reflect other electronic transitions that contribute to the overall Soret absorption.

The absorption spectra for chlorin monomers **C- β AC** and **C- β BTd** also show a feature in the range of 450–460 nm (Figure 1D and E, blue). A feature in this region is also seen in the spectra for the corresponding dyads **C2- β AC** and **C2- β BTd** and for the other dyads (Figure 1, red). The presence of such a feature in the **C- β AC** and **C- β BTd** monomers may reflect (1) strong interaction of the MOs of the linker with those of the chlorin, and/or (2) transitions involving charge-transfer between the chlorin macrocycle and the linker moieties. In this regard, when the spectra are normalized to the total integrated intensity (as is done for Figure 1), the Soret maxima for the **C- β AC** and **C- β BTd** monomers are relatively less intense than for the other chlorin monomers. This suggests some redistribution of intensity from the main Soret bands into the feature in the 450–460 nm spectral region.

The absorption spectra of the chlorin-chlorin dyads (Figure 1, red) differ substantially from the spectra of the individual chlorins. A similar observation was made for the dyads

studied previously (Chart 1) [38], where it was also noted that the traditional band assignments of B_x , B_y , Q_x , and Q_y , are not appropriate due to the strong electronic coupling between the constituents (and possible rotation of the optical axes). Thus, the absorption manifolds of the strongly coupled chlorin-chlorin dyads are denoted B, Q_2 , and Q_1 from higher to lower energy. One of the main differences between the spectra of each dyad and its corresponding monomer in Figure 1 is the splitting of the Q_1 (nominal Q_y) band. The two features are denoted $Q_{1\beta}$ and $Q_{1\alpha}$, progressing from higher to lower energy. For the β -linked chlorin dyads studied here (Chart 2), splitting in the Q_2 (nominal Q_x) band does not appear to be substantial. However, for *meso*-linked analogs studied previously (Chart 1), such splitting in the Q_2 band is comparable to or greater than that in the Q_1 band [38]. The difference reflects the extent of electron density at the linker position of the various frontier MOs (*vide infra*).

The splitting between the $Q_{1\beta}$ and $Q_{1\alpha}$ features for the chlorin dyads is denoted $\Delta\lambda_{Q_1}^{\text{split}}$. The shift in the energy center of gravity of the $Q_{1\beta}$ and $Q_{1\alpha}$ features from the Q_y maximum for the monomer is denoted $\Delta\lambda_{Q_1}^{\text{shift}}$. The values are listed in Table 1 along with the shift $\Delta\lambda_{Q_2}^{\text{shift}}$ in the Q_2 band of a dyad from the Q_x band of the monomer. The value of $\Delta\lambda_{Q_2}^{\text{shift}}$ ranges from $\sim 140 \text{ cm}^{-1}$ to $\sim 375 \text{ cm}^{-1}$ and shows a rough trend with the larger value of $\Delta\lambda_{Q_1}^{\text{shift}}$ that ranges from $\sim 125 \text{ cm}^{-1}$ to $\sim 730 \text{ cm}^{-1}$ (Figure 2A). The splitting between the $Q_{2\beta}$ and $Q_{2\alpha}$ bands ($\Delta\lambda_{Q_1}^{\text{split}}$) is in the range $\sim 200 \text{ cm}^{-1}$ to $\sim 525 \text{ cm}^{-1}$ and varies to some extent with the band shift $\Delta\lambda_{Q_1}^{\text{shift}}$ (Figure 2B).

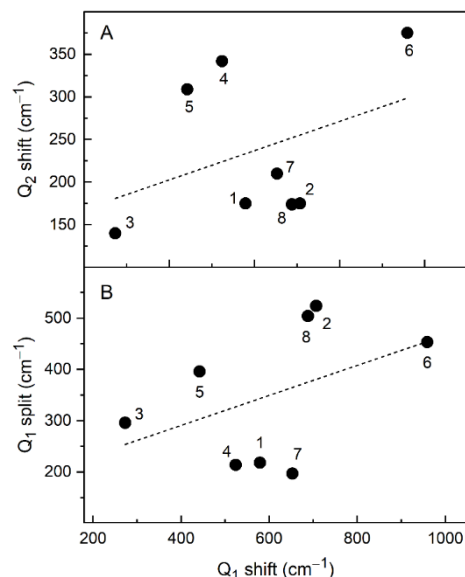


Figure 2. The shift $\Delta\lambda_{Q_2}^{\text{shift}}$ in the Q₂ band of the dyad from the Q_x band of the monomer (A) or the splitting $\Delta\lambda_{Q_1}^{\text{split}}$ between the Q_{1β} and Q_{1α} bands of the dimer (B) versus the shift $\Delta\lambda_{Q_1}^{\text{shift}}$ in the Q₁ band of the dyad from the Q_y band of the monomer. The labels on the points are as follows: **C₂-βBm** (1), **C₂-βEm** (2), **C₂-βP** (3), **C₂-βAC** (4), **C₂-βBTD** (5), **C₂-βV** (6), **C₂-βB** (7), and **C₂-βE** (8). The dashed lines are guides to the eye.

Some physical/electronic factors may influence both $\Delta\lambda_{Q_1}^{\text{split}}$ and $\Delta\lambda_{Q_1}^{\text{shift}}$ whereas others may not. Thus, a correlation between the Q₁ shift and splitting parameters is not necessarily expected. Of the two parameters, $\Delta\lambda_{Q_1}^{\text{split}}$ is the best reflection of the extent of linker-mediated electronic communication between the two chlorins in a dyad. Ultimately, the Q_{1β} – Q_{1α} spectral splitting derives from manner in which electronic interactions within the dyad give rise to pairs (or sets) of MOs that are linear combinations of the corresponding MOs of the constituents (*vide infra*). Such interactions could also affect $\Delta\lambda_{Q_1}^{\text{shift}}$, which ultimately reflects a change in the average energy gap between the filled versus empty orbitals of the dyad relative to that gap in the monomers. The spectral/energy shift parameter $\Delta\lambda_{Q_1}^{\text{shift}}$ also involves a difference in “solvation” of the chlorin macrocycles in the dyad compared to the monomers. Each chlorin monomer is uniformly surrounded by solvent molecules. In the dyad, part of the space around each chlorin is

now taken up by the linker and the other chlorin. This spatial effect gives a difference in the overall dispersive interactions experienced by a chlorin in a dyad versus the monomers. Such effects on $\Delta\lambda_{Q1}^{\text{shift}}$ do not derive simply from the inter-subunit electronic couplings that underlies $\Delta\lambda_{Q1}^{\text{split}}$.

The magnitude of the splitting $\Delta\lambda_{Q1}^{\text{split}}$ between the $Q_{1\beta}$ and $Q_{1\alpha}$ bands of ethynyl-linked dyad **C2- β Em** obtained here (545 cm^{-1}) is comparable to that of the analog **C2- β E** (504 cm^{-1}) studied previously [38]. This is expected because the two dyads differ only in whether each chlorin contains a mesityl (m) versus tolyl group at a non-linking 10-position (Charts 1 and 2). Similarly, $\Delta\lambda_{Q1}^{\text{split}}$ for the butadiynyl-linked dyad **C2- β Bm** (240 cm^{-1}) is comparable to that for **C2- β B** (197 cm^{-1}) previously reported [38]. This comparison reinforces the fact that the shorter ethynyl linker mediates greater electronic communication between the chlorins than the longer butadiynyl linker. It is also interesting to note that the shift $\Delta\lambda_{Q1}^{\text{shift}}$ in the average energy of the split $Q_{1\beta}$ and $Q_{1\alpha}$ bands of the dyad from monomer Q_y are comparable for **C2- β Em**, **C2- β E**, **C2- β Bm** and **C2- β B** (456, 436, 460 and 555 cm^{-1}) and if anything is slightly larger for the butadiynyl versus ethynyl linker. This result may reflect the interplay between the through-bond versus through space-interactions between the chlorins and steric restrictions on the approach of solvent molecules to the chlorin macrocycles.

The energy-minimized structures used in the DFT calculations described below indicate that the vinyl linker in dyad **C2- β V** gives an edge-to-edge distance between chlorins (3.84 Å) that is less than that for **C2- β Em** and **C2- β E** (both 4.04 Å) and the distance for **C2- β Bm** and **C2- β B** (both 6.62 Å). Yet the $\Delta\lambda_{Q1}^{\text{split}}$ splitting value (263 cm^{-1}) for the dyad with the vinyl linker is intermediate between those for the ethynyl and butadiynyl linkers. This shows that additional

factors influence the electronic communication between the two chlorins in the dyad. Such factors include orientation (including torsional motions) and the relative energies of the MOs of the linker and those of the chlorins (*vide infra*). It is of interest that the shift in the average Q_1 energy of **C2- β V** from the Q_y energy in the **C- β V** monomer ($\Delta\lambda_{Q_1}^{\text{shift}} = 710 \text{ cm}^{-1}$) is the largest of all the dyads (Table 1). This could arise in part from the close separation of the two units and thus the greatest perturbation to the uniform solvation experienced by the chlorin constituents of this dyad versus the chlorin monomer.

Three of the new dyads have a spacing between chlorins that is larger than provided by the butadiyne linker due to the presence of an aromatic ring system between the two ethyne groups. The linker in these three dyads contain a dialkoxy-phenyl group (**C2- β P**), a benzothiadiazole unit (**C2- β BTd**) or an anthracenyl group (**C2- β AC**), as shown in Chart 2. The magnitude of the splitting $\Delta\lambda_{Q_1}^{\text{split}}$ increases in the order **C2- β P** (180 cm^{-1}) < **C2- β AC** (277 cm^{-1}) < **C2- β BTd** (375 cm^{-1}) (Table 1 and Figure 2). There seems to be no correlation with the $\Delta\lambda_{Q_1}^{\text{shift}}$ values, which increase with the size of the ring system in the order **C2- β P** (205 cm^{-1}) < **C2- β BTd** (233 cm^{-1}) < **C2- β AC** (427 cm^{-1}). It is noteworthy that the presence of the anthracenyl group in the linker of **C2- β AC** results in Q_1 splitting $\Delta\lambda_{Q_1}^{\text{split}}$ (222 cm^{-1}) that is larger than that for the butadiynyl linker of **C2- β Bm** (240 cm^{-1}) and **C2- β B** (197 cm^{-1}) despite the fact that the aromatic group increases the spacing between the two chlorins. The origin of this difference is discussed below in terms of MO characteristics.

B. Fluorescence Emission Spectra. Figure 1 shows the room temperature fluorescence spectra of chlorin dyads (dashed red) and the benchmark monomers (dashed blue) in toluene. The peak wavelength and full-width-at-half-maximum (fwhm) of each compound are listed in

Table 1. Similar spectra are observed in benzonitrile (Figure S1). The fluorescence from each dyad is dominated by the $Q_{1\alpha}$ band origin, and the vibronic progression to longer wavelength is far weaker. Thus, the emission spectrum is not mirror symmetric to the absorption spectrum, which shows the $Q_{1\alpha}$ band and the $Q_{1\beta}$ feature/shoulder at higher energy. These observations reaffirm that $Q_{1\alpha}$ absorption reflects the $S_0 \rightarrow S_1$ transition and $Q_{1\beta}$ involves excitation to a different electronic state ($S_0 \rightarrow S_2$) and is not a vibronic component of $S_0 \rightarrow S_1$.

The $Q_{1\alpha}$ fluorescence maximum of each dyad is shifted bathochromically from the Q_y fluorescence peak of the benchmark monomer in proportion to the bathochromic shift of the $Q_{1\alpha}$ absorption band of the dyad relative to the Q_y absorption band of the monomer. The Stokes shift between $Q_{1\alpha}$ absorption band and the $Q_{1\alpha}$ fluorescence maximum of the dyads is generally <5 nm. A larger Stokes shift of 10 nm is observed for zinc chelate **ZnC₂- β V**. The small Stokes shifts indicate that the rearrangement of the dyad molecular structure and the reorientation of solvent molecules are minimal in the S_1 state versus the S_0 ground state. The Stokes shifts are larger for some of dyads in the more polar solvent benzonitrile, likely reflecting increases solvent reorientation following excitation (Table S1). The fwhm of the emission from the dyads in toluene is 12-14 nm for **C₂- β Bm**, **C₂- β B**, **C₂- β Em**, and **C₂- β E**. The value increases to 18-21 nm for **C₂- β AC**, **C₂-BTD** and **C₂- β V**, and to 26 nm zinc chelate **ZnC₂- β V** in toluene (Table 1). The fwhm typically increase by ~20% in benzonitrile, and by a larger percentage to 37 nm for **ZnC₂- β V** in the more polar solvent (Table S1).

C. Singlet Excited-State Lifetime and Decay-Pathway Yields/Rate Constants. Table 2 summarizes the photophysical properties of the S_1 state of the chlorin dyads and benchmarks in toluene or benzonitrile. The measured quantities are the singlet excited-state lifetime (τ_s), the quantum yield for $S_1 \rightarrow S_0$ fluorescence (Φ_f) and the quantum yield for $S_1 \rightarrow T_1$ intersystem

crossing (Φ_{isc}), the latter often called the triplet yield. The yield of $S_1 \rightarrow S_0$ internal conversion (Φ_{ic}) is calculated using the formula $\Phi_{ic} = 1 - \Phi_f - \Phi_{isc}$. The corresponding rate constants for the three decay processes of the S_1 excited state k_f , k_{isc} and k_{ic} are obtained using the expression $k_x = \Phi_x / \tau_s$, where $x = f, ic$ or isc . The last three columns of Table 2 gives the inverse values of the rate constants, namely the time constants $(k_x)^{-1}$ in nanoseconds.

Table 2. Singlet Excited–State Properties of Chlorin Dyads.^a

Compound	Solvent	τ_s (ns)	Φ_f	Φ_{isc}	Φ_{ic}	$(k_f)^{-1}$ (ns)	$(k_{isc})^{-1}$ (ns)	$(k_{ic})^{-1}$ (ns)
<i>Current Dyads</i>								
C₂-βBm	toluene	5.2	0.61	0.27	0.12	8.5	19	43
	benzonitrile	4.6	0.48	0.24	0.28	9.6	19	16
C₂-βEm	toluene	5.0	0.54	0.28	0.18	9.3	18	28
	benzonitrile	4.7	0.48	0.28	0.24	9.8	17	20
C₂-βP	toluene	6.7	0.47	0.34	0.19	14	20	35
	benzonitrile	6.0	0.44	0.33	0.23	14	18	26
C₂-βAC	toluene	4.2	0.52	0.22	0.26	8.1	19	16
	benzonitrile	3.3	0.37	0.18	0.45	8.9	18	7.3
C₂-βBTD	toluene	4.4	0.59	0.31	0.10	7.5	14	44
	benzonitrile	1.3	0.16	0.10	0.74	8.1	14	1.7
C₂-βV	toluene	3.7	0.43	0.25	0.32	8.6	15	12
	benzonitrile	3.4	0.40	0.23	0.37	8.5	15	9.2
ZnC₂-βV	toluene	2.2	0.25	0.33	0.42	8.8	6.7	5.2
	benzonitrile	1.3	0.15	0.22	0.63	8.7	5.9	2.1
<i>Prior Dyads</i>								
C₂-βB	toluene	5.7	0.57	0.29	0.14	10	20	41
	benzonitrile	5.0	0.52	0.25	0.23	9.6	20	22
C₂-βE	toluene	5.2	0.48	0.25	0.27	11	21	19
	benzonitrile	4.8	0.40	0.30	0.30	12	16	16
<i>Current Benchmark Monomers</i>								
C-βEm	toluene	8.3	0.40	0.54	0.060	21	15	138
	benzonitrile	7.9	0.37	0.54	0.090	21	14	88
C-βAC	toluene	7.6	0.39	0.41	0.20	19	19	38
	benzonitrile	7.1	0.35	0.43	0.22	20	17	32
C-βBTD	toluene	7.7	0.58	0.42	0.01	13	18	>150 ^b
	benzonitrile	7.3	0.41	0.44	0.15	18	17	49
C-βV	toluene	7.4	0.42	0.52	0.06	18	14	123
	benzonitrile	7.3	0.38	0.52	0.10	19	14	73
<i>Prior Benchmark Monomers</i>								
C-βB	toluene	9.3	0.34	0.50	0.16	27	19	58
	benzonitrile	9.1	0.31	0.50	0.19	29	18	48
C-βE	toluene	8.8	0.39	0.55	0.060	23	16	147
	benzonitrile	8.5	0.36	0.48	0.16	24	18	53

^aThe typical errors (percent of value) are τ_s ($\pm 5\%$), Φ_f ($\pm 5\%$), Φ_{isc} ($\pm 10\%$), Φ_{ic} ($\pm 15\%$), k_f ($\pm 10\%$), k_{isc} ($\pm 15\%$), k_{ic} ($\pm 20\%$). ^bLower limit based on experimental error.

The Φ_f values of the free base chlorin dyads in toluene are in the range 0.43–0.61, in all cases but one being substantially larger than the values for the corresponding benchmark monomers in toluene (0.34–0.61). For example, the Φ_f of 0.54 for dyad **C₂-βEm** is ~25% larger than the value of 0.40 for monomer **C-βEm** in toluene. The exception is that Φ_f is comparable for dyad **C₂-βBTD** (0.59) and monomer **C-βBTD** (0.58) in toluene. The similar fluorescence yields for this dyad and monomer are fortuitous, because the singlet lifetime for dyad **C₂-βBTD** in toluene (4.4 ns) is substantially shorter than that for monomer **C-βBTD** (7.7 ns). These results reflect the composite effect of the rate constants for the three S₁ excited-state decay pathways (*vide infra*).

For the dyads in general, the fluorescence yield is lower and the singlet lifetime is shorter in benzonitrile than in toluene (Table 2). For example, the Φ_f and τ_s values in benzonitrile / toluene are (0.48, 4.7 ns) / (0.54, 5.0 ns) for **C₂-βEm**, (0.40, 3.4 ns) / (0.43, 3.7 ns) for **C₂-βV**, (0.44, 6.0 ns) / (0.47, 6.7 ns) for **C₂-βP**, (0.37, 3.3 ns) / (0.52, 4.2 ns) for **C₂-βAC**, and (0.16, 1.3 ns) / (0.59, 4.4 ns) for **C₂-βBTD**. It can be seen that the most substantial solvent dependence is observed for **C₂-βBTD**. Although reductions in Φ_f and τ_s values are also observed for the companion monomers in benzonitrile versus toluene, the magnitude of the solvent dependence is less than for the dyads. For example, the Φ_f and τ_s values in benzonitrile / toluene are (0.37, 7.9 ns) / (0.40, 8.3 ns) for **C-βEm**, (0.38, 7.3 ns) / (0.42, 7.4 ns) for **C-βV**, (0.35, 7.1 ns) / (0.39, 7.6 ns) for **C-βAC**, and (0.41, 7.3 ns) / (0.58, 7.7 ns) for **C-βBTD**.

The Φ_f and τ_s values for **ZnC₂-βV** in benzonitrile / toluene of (0.15, 1.3 ns) / (0.25, 2.2 ns) are all significantly decreased from those for **C₂-βV** in benzonitrile / toluene of (0.40, 3.4 ns) / (0.43, 3.7 ns). As will be discussed below, these differences in both solvents can be traced to increased rate constants for both the intersystem crossing and internal conversion decay pathways of the zinc chelate versus the free base form of the vinyl-linked dyad.

The Φ_{isc} values for the chlorin dyads in toluene (0.22–0.34) are smaller than those for the benchmarks (0.41–0.55) (Table 2). For example, the values in toluene are 0.28 vs 0.54 for **C2- β Em** vs **C- β Em**, 0.25 vs 0.52 for **C2- β V** vs **C- β V**, 0.22 vs 0.41 for **C2-AC** vs **C-AC**, and 0.31 vs 0.42 for **C2- β BTD** vs **C- β BTD**. It can be seen that the least reduction in Φ_{isc} for a dyad versus the monomer is for the benzothiadiazole (BTD) linker. Generally similar reductions in Φ_{isc} values are observed for the dyads versus the monomers in benzonitrile. For most dyads, Φ_{isc} is comparable in toluene and benzonitrile. The most substantial solvent polarity dependence is observed for **C2- β BTD**, for which Φ_{isc} is 0.31 in toluene and 0.095 in benzonitrile. Dyad **ZnC2- β V** has a Φ_{isc} value of 0.33 in toluene and 0.22 in benzonitrile, showing a smaller solvent dependence than **C2- β BTD** but larger than the other dyads.

The Φ_{ic} values for the chlorin dyads in toluene are larger than those for the benchmarks. For example, values in toluene are 0.18 vs 0.06 for **C2- β Em** vs **C- β Em**, 0.32 vs 0.06 for **C2- β V** vs **C- β V**, 0.26 vs 0.20 for **C2-AC** vs **C-AC**, and 0.10 vs <0.05 for **C2- β BTD** vs **C- β BTD**. The Φ_{ic} values in benzonitrile are 0.24 vs 0.09 for **C2- β Em** vs **C- β Em**, 0.37 vs 0.10 for **C2- β V** vs **C- β V**, 0.45 vs 0.22 for **C2-AC** vs **C-AC**, and 0.75 vs 0.15 for **C2- β BTD** vs **C- β BTD**. It can be seen that the most substantial difference in Φ_{ic} between the two solvents is for dyad **C2- β BTD** (0.75 in benzonitrile versus 0.10 in toluene). The next largest differences between benzonitrile and toluene are for **C2- β AC** (0.45 versus 0.26) and **ZnC2- β V** (0.63 versus 0.42).

All the differences in the measured singlet excited-state lifetime (τ_s) and the quantum yields for the three decay pathways (Φ_f , Φ_{isc} , and Φ_{ic}), inherently derive from the combined values of the associated rate constants for $S_1 \rightarrow S_0$ fluorescence (k_f), $S_1 \rightarrow T_1$ intersystem crossing (k_{isc}), and $S_1 \rightarrow S_0$ internal conversion (k_{ic}). The values are listed in the last three columns of Table 2 as the corresponding time constant in units of nanoseconds. It bears

reminding that the inverse of each rate constant is the lifetime (decay time constant) that would be measured if that process was the sole pathway for decay of the S_1 state of the molecule. In that vein, $\tau_f = 1/k_f$ is often referred to as the natural radiative lifetime, being distinct from the measured lifetime τ_s .

The k_f values are roughly two-fold larger (the k_f^{-1} values are roughly two-fold smaller) for the dyads than those for the monomers. For example, the values in toluene are $(9.3 \text{ ns})^{-1}$ vs $(21 \text{ ns})^{-1}$ for **C₂- β Em** vs **C- β Em**, $(8.6 \text{ ns})^{-1}$ vs $(18 \text{ ns})^{-1}$ for **C₂- β V** vs **C- β V**, $(8.1 \text{ ns})^{-1}$ vs $(19 \text{ ns})^{-1}$ for **C₂-AC** vs **C-AC**, and $(7.5 \text{ ns})^{-1}$ vs $(13 \text{ ns})^{-1}$ for **C₂- β BTd** vs **C- β BTd**. The k_{isc} values for all dyads and benchmarks (except for **ZnC₂- β V**) in toluene and benzonitrile are in the narrow range of $(14\text{--}21 \text{ ns})^{-1}$. Intersystem crossing for **ZnC₂- β V** of [$k_{isc} = (5.9\text{--}6.7 \text{ ns})^{-1}$] is increased relative to that for **C₂- β V** of [$k_{isc} = (8.5\text{--}8.6 \text{ ns})^{-1}$] due to heavy-atom enhancement of spin-orbit coupling [46] involving the central zinc ion.

The k_{ic} values for the dyads are generally substantially larger than those for the monomers, even considering that the (compound) error in these values is the largest of all the excited-state parameters (Table 2). For example, the values in toluene are $(28 \text{ ns})^{-1}$ vs $(138 \text{ ns})^{-1}$ for **C₂- β Em** vs **C- β Em**, $(12 \text{ ns})^{-1}$ vs $(123 \text{ ns})^{-1}$ for **C₂- β V** vs **C- β V**, $(16 \text{ ns})^{-1}$ vs $(38 \text{ ns})^{-1}$ for **C₂-AC** vs **C-AC**, and $(44 \text{ ns})^{-1}$ vs $(>150 \text{ ns})^{-1}$ for **C₂- β BTd** vs **C- β BTd**. For comparison, the k_{ic} values benzonitrile are $(20 \text{ ns})^{-1}$ vs $(87 \text{ ns})^{-1}$ for **C₂- β Em** vs **C- β Em**, $(9.2 \text{ ns})^{-1}$ vs $(73 \text{ ns})^{-1}$ for **C₂- β V** vs **C- β V**, $(7.3 \text{ ns})^{-1}$ vs $(32 \text{ ns})^{-1}$ for **C₂-AC** vs **C-AC**, and $(1.7 \text{ ns})^{-1}$ vs $(49 \text{ ns})^{-1}$ for **C₂- β BTd** vs **C- β BTd**. One contributor to enhanced internal conversion in the dyads versus monomers involves motions of the dyad that alter the spatial relationship of the two chlorins with respect to the linker and each other, especially if they alter the electronic character of the dyad (*vide infra*). The energy-gap law for non-radiative decay [46] would predict enhanced internal

conversion for the dyads owing to the lower energy excited state compared to the monomers, as manifested by the bathochromic shift in the $Q_{1\alpha}$ band of the dimer from the Q_y band of the monomer (Figure 1 and Table 1).

A final comparison of internal conversion rates involves **ZnC₂-βV** [$k_{ic} = (5.2 \text{ ns})^{-1}$ in toluene and $(2.1 \text{ ns})^{-1}$ in benzonitrile] versus **C₂-βV** [$k_{ic} = (12 \text{ ns})^{-1}$ in toluene and $(9.2 \text{ ns})^{-1}$ in benzonitrile]. Faster internal conversion in the zinc chelate versus the free base form in toluene is unexpected. [Internal conversion is faster still for the zinc chelate versus the free base form in benzonitrile, but axial ligation of the metal and associated structural/electronic effects could play a role in this solvent]. The energy-gap law would predict the reverse, namely a slower internal conversion for **ZnC₂-βV** because it has a higher energy S_1 excited state ($Q_{1\alpha}$ absorption 696 nm and emission 706 nm) than **C₂-βV** ($Q_{1\alpha}$ absorption 707 nm and emission 712 nm). Furthermore, one might have expected that the high-energy N-H vibrations involving the central protons to enhance internal conversion of the free base form versus the zinc chelated. This unexpected dichotomy has been discussed recently in comparative studies of set of simple zinc and free base porphyrins in the number of meso-phenyl substituents is increased from 1–4 [47].

D. Redox Properties. The redox potentials for the chlorins are listed in Table 3. The potentials for the first oxidation/reduction (E_{ox1}/E_{red1}) for most benchmark chlorins are consistent with those reported values for other monomeric chlorins [48]. Values for **C₂-βBTD** and **C₂-βV** could not be obtained because of low solubility (and aggregation) in the medium employed for the redox studies.

Table 3. Redox Properties of Chlorin Dyads.^a

Compound	E _{ox1} (V)	E _{red1} (V)
<i>Current Dyads</i>		
C₂-βBm	+0.58	−1.38, −1.45
C₂-βEm	+0.61, +0.51	−1.44, −1.55
C₂-βP	+0.59	−1.41 ^b
C₂-βAC	+0.63	−1.28, −1.37
C₂-βBTD	N/A ^c	N/A ^c
C₂-βV	+0.69 ^d , +0.58 ^d , +0.52	−1.36 ^d , −1.42, −1.56
ZnC₂-βV	N/A ^c	N/A ^c
<i>Prior Dyads</i>		
C₂-βB	+0.58 ^b	−1.38, −1.45
C₂-βE	+0.61, +0.51	−1.44, −1.55
<i>Current Benchmark Monomers</i>		
C-βEm	+0.55	−1.53
C-βAC	+0.61	−1.41
C-βBTD	+0.64	−1.28 ^d , −1.39
C-βV	+0.65, +0.52	−1.51
<i>Prior Benchmark Monomers</i>		
C-βB	+0.61	−1.45
C-βE	+0.55	−1.53

^aAll potentials (measured in V) were measured on compounds in butyronitrile containing 0.1 M tetrabutylammonium hexafluorophosphate. The potentials are adjusted so that the ferrocene couple has a value of 0.190 V under the conditions of the measurement. ^bWaves broader than those of the monomers. ^cNo redox peaks were observed, possibly due to low solubility or aggregation. ^dShoulder on the main feature.

The most distinct difference in the redox characteristics of the dyads versus monomers is that the former (in most cases) exhibit doubled redox waves. In particular, the first reduction wave for all the dyads except **C₂-βP** exhibits two resolved or partially resolved features at the potentials listed in Table 4. The reduction wave for **C₂-βP** is broader than that of the monomer, suggesting two underlying features. Similarly, the first oxidation wave for most dyads are either doubled or are broader than those for the monomers, again suggesting two underlying features. The redox properties of dyads **C₂-βBTD** (and **ZnC₂-βV**) could not be measured due to low

solubility (and/or aggregation). We note that the reduction of monomer **C-βBTD** has two apparent contributions, one of which could involve the benzothiadiazole unit. In summary, the observation of split redox waves in the dyads is direct evidence for strong linker-mediated electronic coupling between the two constituent hydroporphyrins in the ground electronic state.

E. Structural Characteristics. DFT calculations were performed on the dyads and benchmarks, starting with the optimized molecular geometry. Exploration of the structural characteristics of the dyads is described in Supplemental Information. Key aspects are summarized here. The β-linked dyad **C₂-βEm**, like **C₂-βE** studied previously [38], has a minimum energy structure with the chlorin macrocycles coplanar in an *anti*-conformation (i.e. substituents on chlorin are located on the opposite sites with respect to the linker, Chart 2). The barrier to internal rotation about the ethyne linker is quite low (<1.5 kcal/mol), consistent with previous calculations^{35,49} on the same or similar dyads. The barrier is smaller (≤0.5 kcal/mol) for dyad **C₂-βBm**, like analog **C₂-βB** studied previously [38]. The low barrier allows the dyad to sample essentially the full space of internal rotational conformations at room temperature. Dyads **C₂-βV** and **C₂-βP** have a minimum near the *anti*-conformation while **C₂-βAC** and **C₂-βBTD** have a minimum near the *syn*-conformation. The torsional barriers for **C₂-βAC** is low (<1.5 kcal/mol) like those for **C₂-βE** and **C₂-βB**. The barriers for **C₂-βBTD** (~3 kcal/mole), **C₂-βP** (~4 kcal/mole) and **C₂-βV** (~ 5 kcal/mol) are progressively larger (Figure S2). A relatively large torsional barrier for **C₂-βV** may reflect the fact that rotations around the single bond between one of the two chlorins and the vinyl linker that remove the two chlorins from an approximate coplanar arrangement effectively reduce conjugation involving the vinyl group. Steric interactions involving the alkoxy-like substituents on the central phenyl ring of **C₂-βP** could constrain torsional motions. The anthracene unit in the linker of **C₂-βAC** is twisted ~20–22° from the plane(s) of the chlorins (Figure S3). The lowest energy structure for **C₂-**

βBTD has a *syn*-conformation in which the benzotriazole (BTD) ring is flipped so that there is a short (3.14 Å) distance, and potential hydrogen-bonding (or other non-covalent) interaction, between a BTD nitrogen atom and the nearby hydrogen atom at the 15-position of the adjacent chlorin (Figure S4). Such interactions could constrain rotation of the chlorins with respect to the linker and contribute to the narrower long-wavelength absorption manifold of **C₂-βBTD** compared to that for **C₂-βAC** (Figure 1E versus 1D).

F. MO Characteristics. Figures 3–8 show the MO distributions and energies of the frontier MOs for the new dyads (Chart 2). Analysis of these diagrams is aided by Figure 9, which illustrates that the frontier MOs of a dyad are linear combinations of monomer MOs due to strong linker-mediated interactions [50,51]. Within each pair, the dyad MOs are labeled with superscript ‘l’ (lower energy) and ‘h’ (higher energy) on the appropriate monomer orbital (e.g., LUMO^l and LUMO^h for the dyad MOs originating from the LUMO of the two monomers). Figure 9 also shows the allowed (for coplanar chlorins in an *anti*-configuration) one-electron promotions analogous to those for the benchmarks within the four-orbital model [4–6]. Table 4 summarizes the splitting within the pair of dyad HOMOs and the splitting of the pair of dyad LUMOs along with other parameters such as the edge-to-edge distance between chlorins. Table 5 summarizes the energies of the frontier MOs for the benchmark chlorins and linkers. Such relative energies contribute to the chlorin-linker interactions (*vide infra*).

A question may arise as the extent to which the electronic communication in these dyads and associated pairs (or sets) of MOs that are linear combinations of the corresponding MOs of the monomers result from (1) through space interactions between chlorins and (2) linker-mediated interactions between the chlorins. This issue was examined by performing calculations for fictive dyads **C₂βE0** and **C₂βV0** in which the ethyne or vinyl linker, respectively, was removed but the structure was frozen at the optimized geometry of the actual dyads **C₂βE** and

C₂βV, respectively. Figures S5 and S6 show that the MOs of the dyad are no longer split and have energies very close to those of the benchmark chlorins. These results demonstrate that the MO properties of the dyads shown in Figures 3-6 and summarized in Table 4 result basically entirely from linker-mediated interactions. This conclusion is consistent with the finding that for certain dyads the MOs of the dyad reveal substantial mixing MOs of the linker with those of the chlorin constituents, giving electron density spread across the entire molecule (*vide infra*).

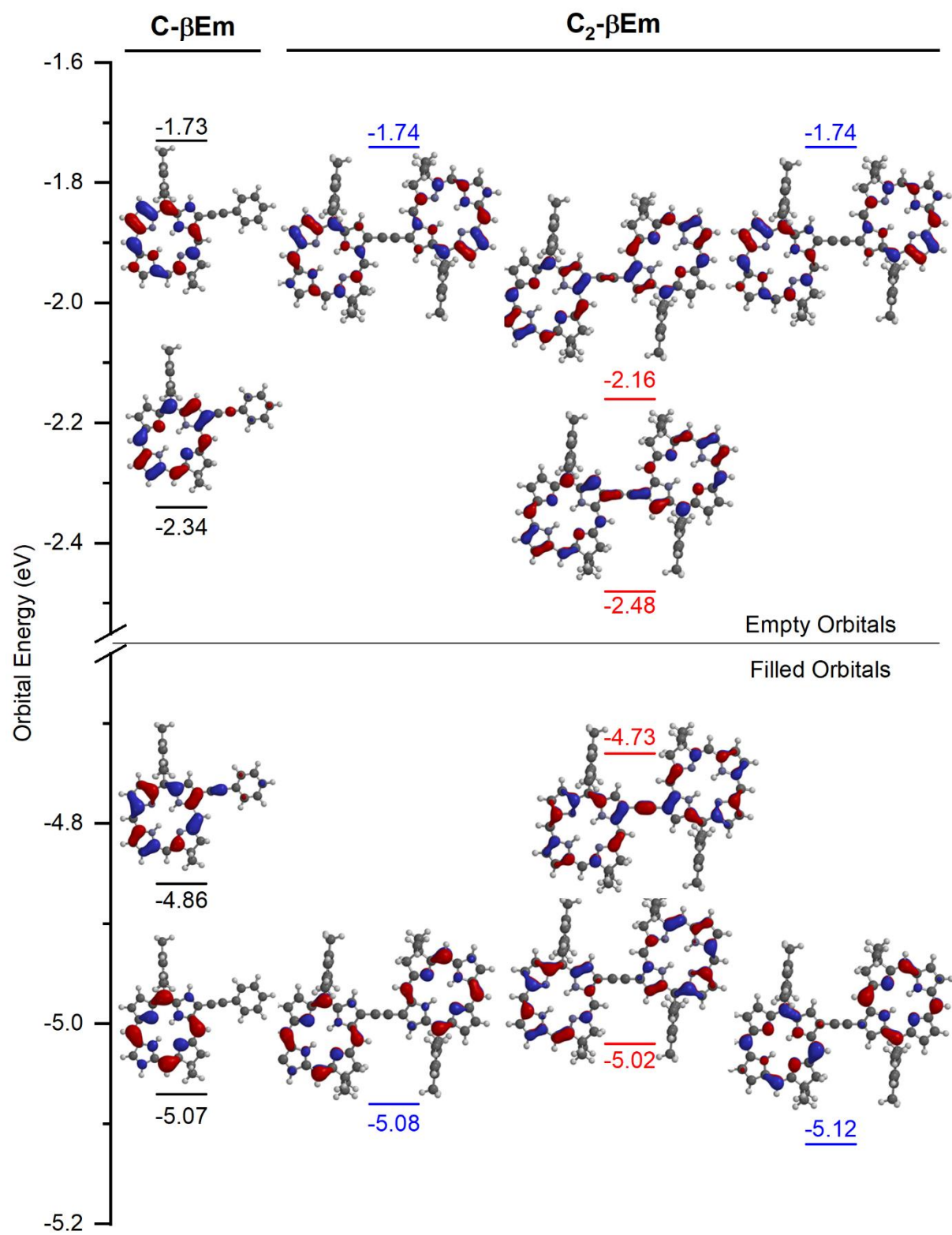


Figure 3. Frontier MOs and MO energy levels of **C₂-βEm** and benchmark chlorin **C-βEm**. Color-coding: red, orbitals that are a mixture of the chlorin HOMO or LUMO and linker HOMO or LUMO; blue, orbitals that are primarily chlorin HOMO or LUMO.

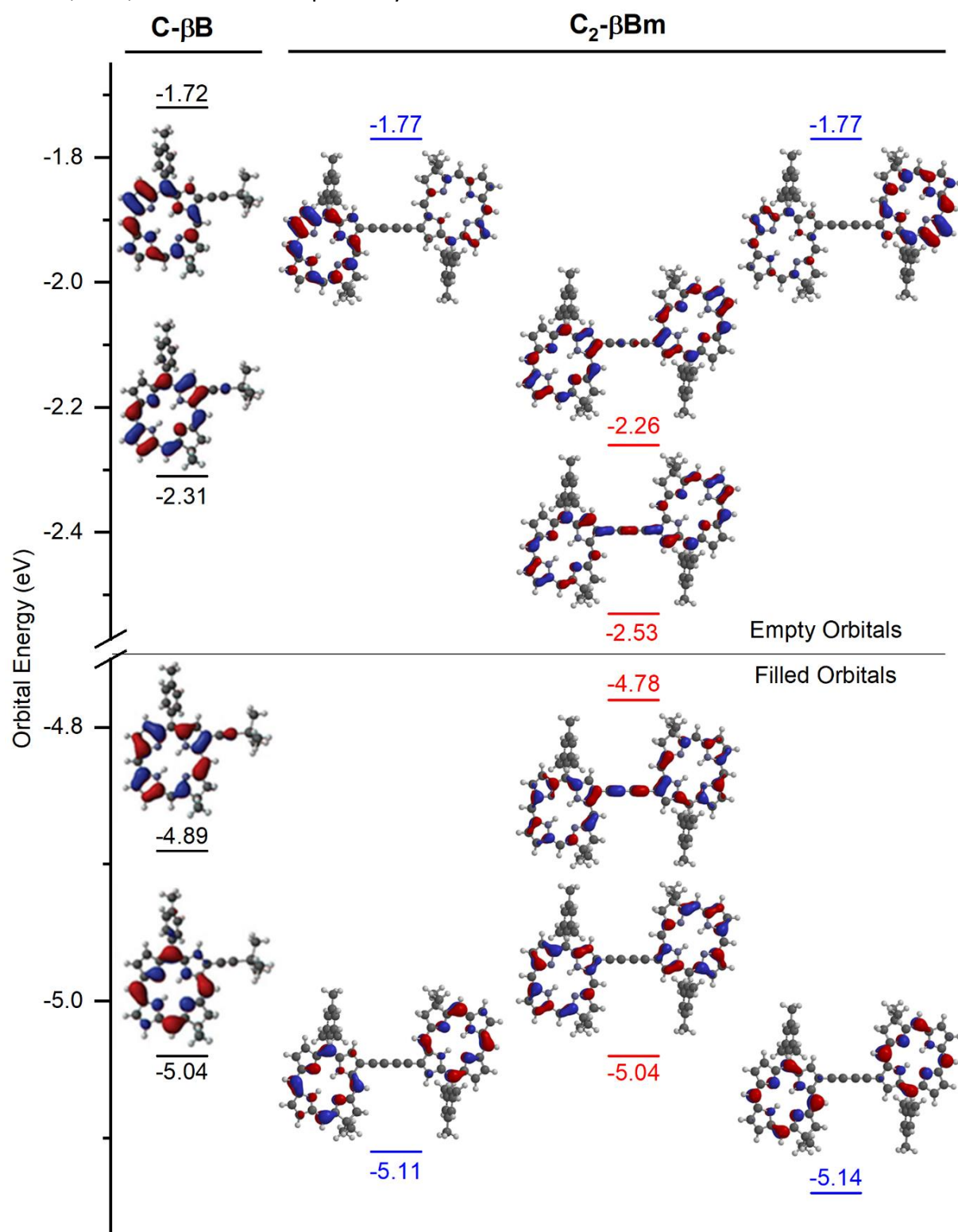


Figure 4. Frontier MOs and MO energy levels of **C₂-βBm** and benchmark chlorin **C-βB**. The color-coding is as in **Figure 3**.

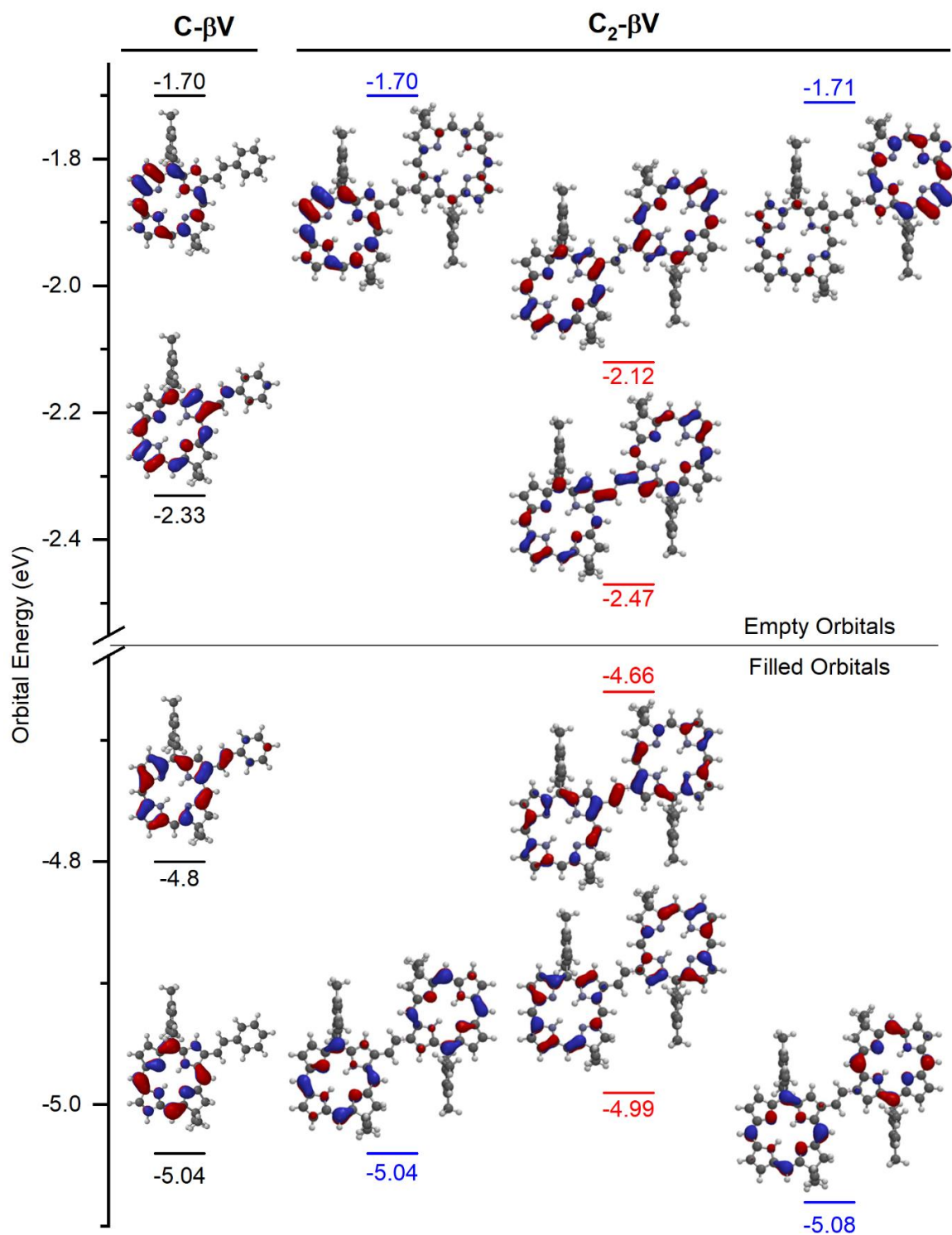


Figure 5. Frontier MOs and MO energy levels of **C₂-βV** and benchmark chlorin **C-βV**. The color-coding is as in **Figure 3**.

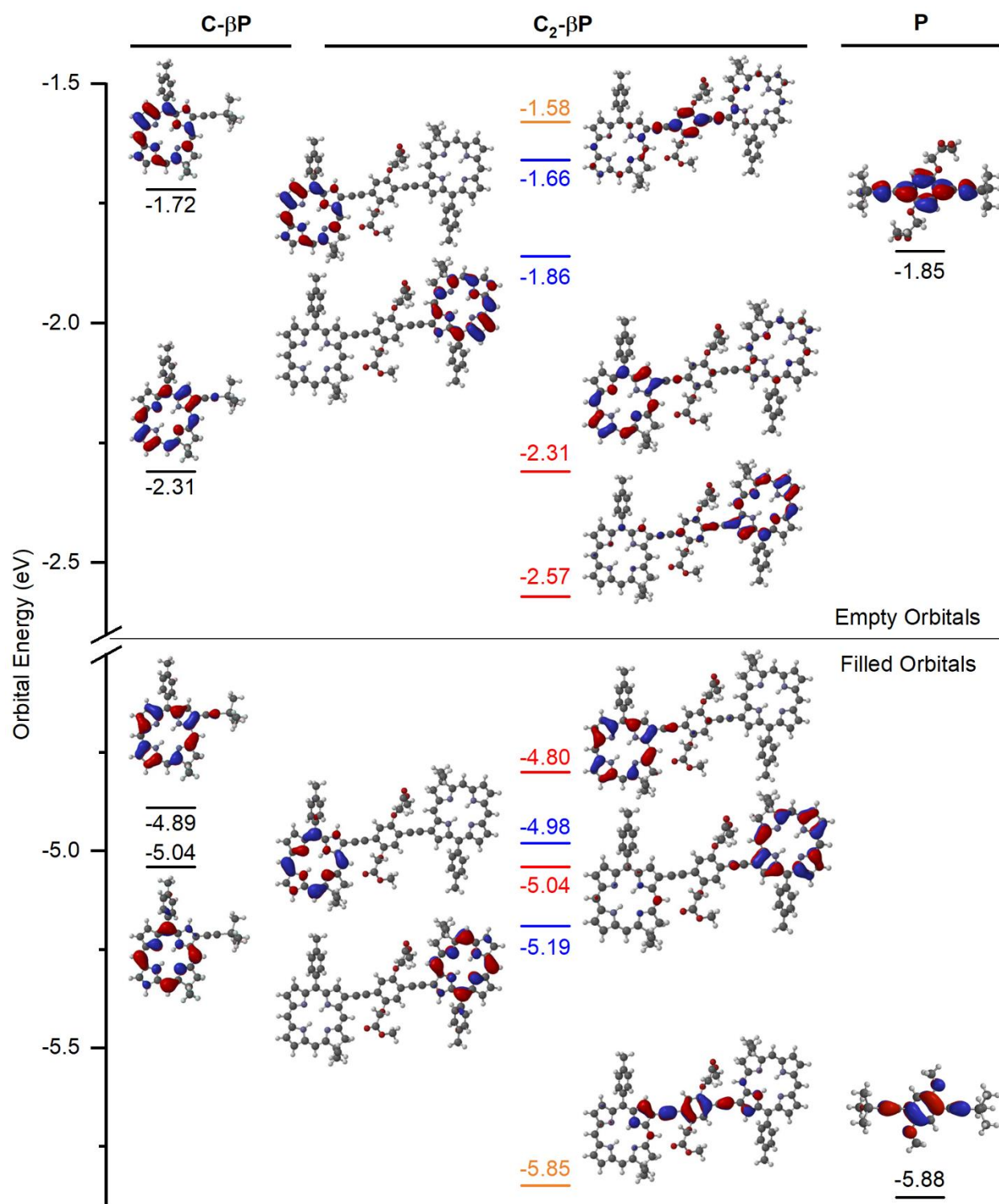


Figure 6. Frontier MOs and MO energy levels of **C₂-βP**, benchmark chlorin **C-βB**, and benchmark **P** linker. The color-coding is as in Figure 3. See Figure S5 for the MO diagram for the fictive analog **C₂-βP0** that lacks the alkoxy-like substituents on the linker.

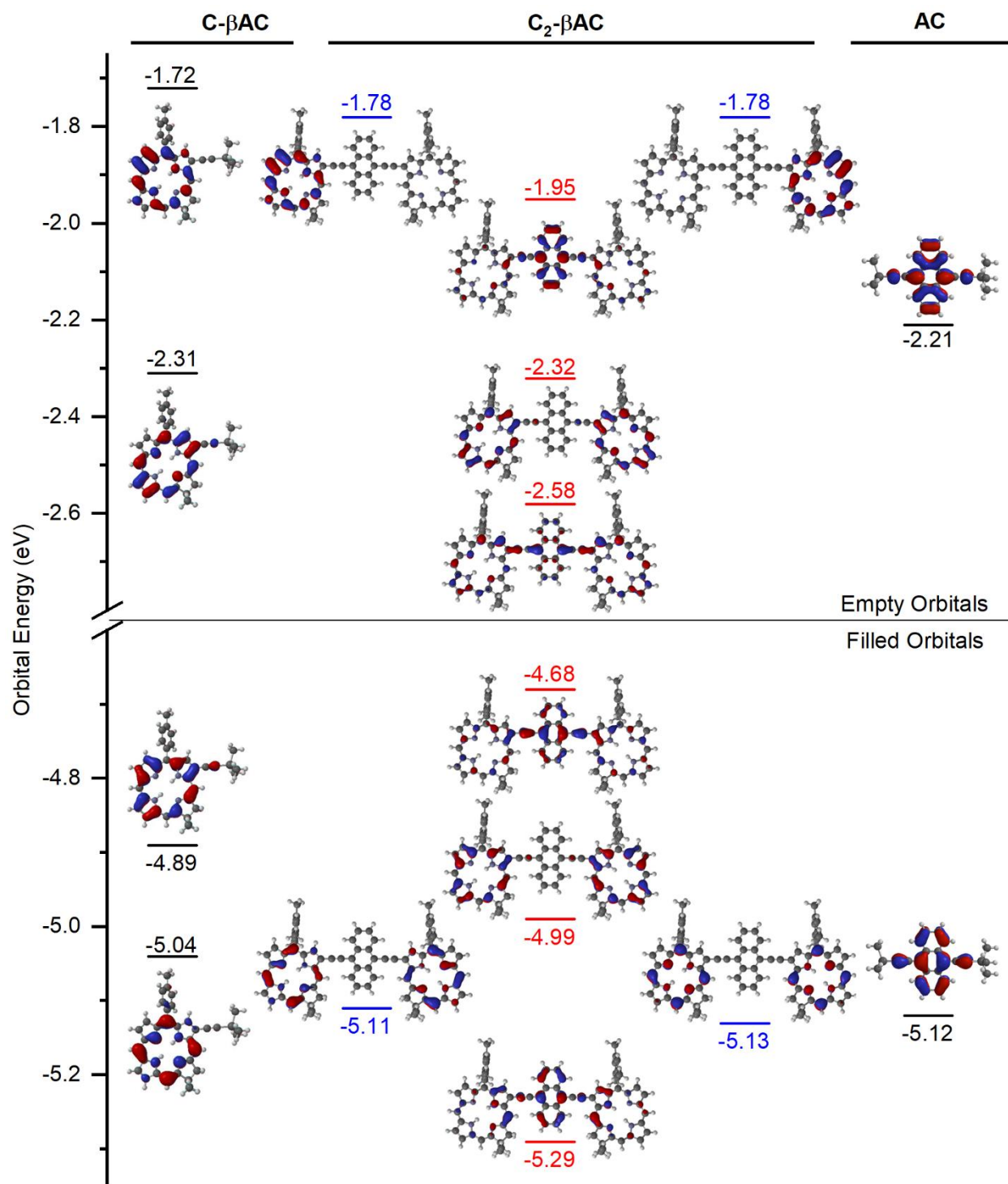


Figure 7. Frontier MOs and MO energy levels of **C₂-βAC**, benchmark chlorin **C-βB**, and benchmark **AC** linker. The color-coding is as in Figure 3.

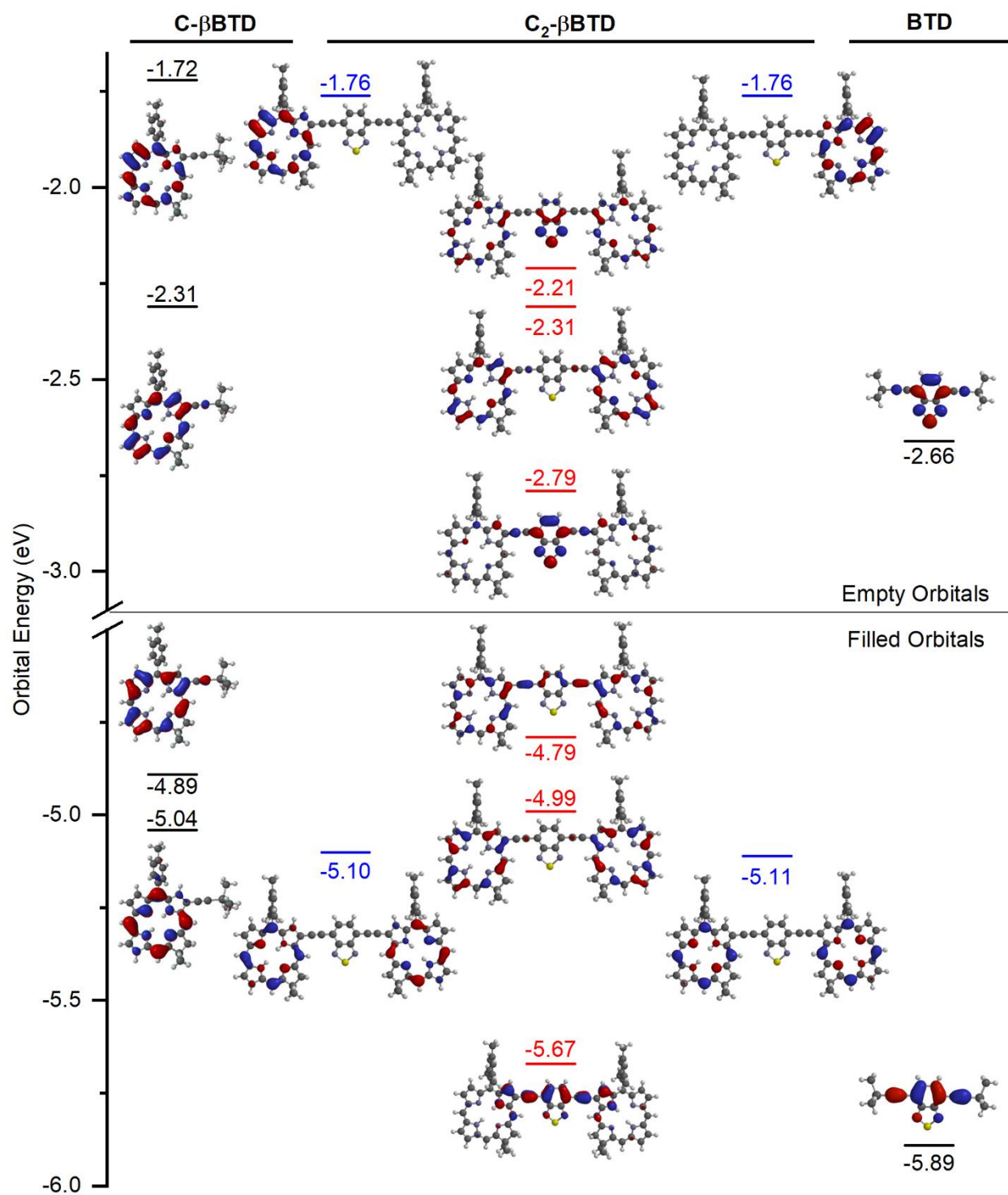


Figure 8. Frontier MOs and MO energy levels of C₂-βBTD, benchmark chlorin C-βB, and benchmark BTD linker. The color-coding is as in Figure 3.

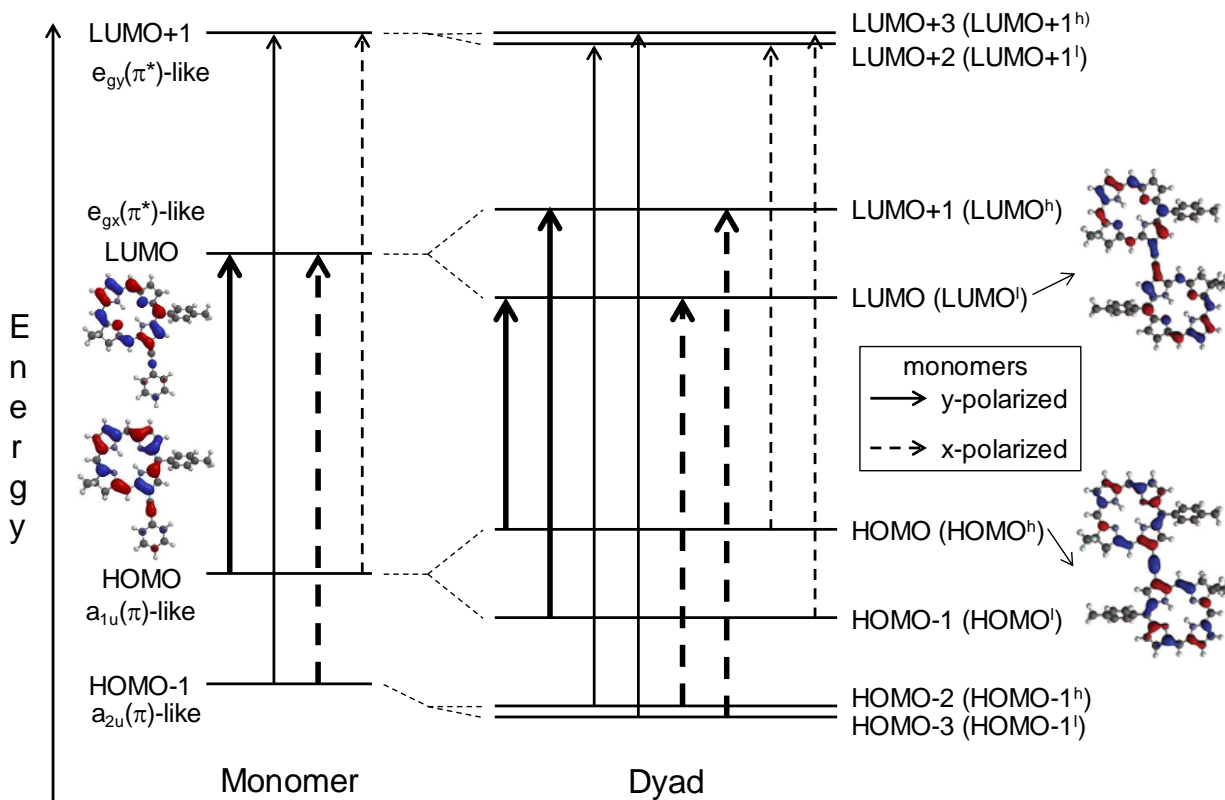


Figure 9. Nomenclature for the frontier MOs of a chlorin monomer and the linear combinations that are the frontier MOs of a dyad. In this example, there is less linker-mediated splitting of dyad MOs derived from interacting HOMO-1 of the monomers or interacting LUMO+1 of the monomers compared to the interacting monomer HOMOs and interacting monomer LUMOs. For this illustration, the MOs primarily derived from the linker HOMO and LUMO are outside the energy regime shown. The diagram also shows representative allowed one-electron promotions of the dyads assuming coplanar macrocycles in a *anti*-configuration (C_{2h} symmetry). For the monomers, the solid and dashed arrows indicate the y- and x-axis promotions, respectively. This illustration is relevant to chlorin dyads **C₂-βEm**, **C₂-βBm**, and **C₂-βV**.

Table 4. MO characteristics of dyads.

Quantity	C2-βBm	C2-βB	C2-βEm	C2-βE	C2-βV	C2-βP	C2-βP0^h	C2-βAC	C2-βBTD
Distance (Å) ^a	6.615	6.615	4.036	4.036	3.840	10.943	10.927	10.935	10.927
LUMO ^h (eV) ^b	-2.26	-2.24	-2.16	-2.15	-2.12	-2.31	-2.29	-1.95 ^c	-2.21
LUMO ^l (eV) ^b	-2.53	-2.50	-2.48	-2.45	-2.47	-2.57	-2.45	-2.58	-2.79
HOMO ^h (eV) ^b	-4.78	-4.75	-4.73	-4.71	-4.66	-4.80	-4.78	-4.68	-4.79
HOMO ^l (eV) ^b	-5.04	-5.02	-5.02	-5.00	-4.99	-5.04	-4.95	-5.29	-5.67
ΔLUMO (eV) ^c	0.27	0.26	0.32	0.30	0.35	0.26	0.16	0.63 ^f	0.58 ^f
ΔHOMO (eV) ^d	0.26	0.27	0.29	0.29	0.33	0.24	0.17	0.61 ^f	0.88 ^f
Avg ΔMO ^e	0.265	0.265	0.305	0.295	0.34	0.25	0.165	0.62	0.73
Q _{1β} – Q _{1α} (meV) ^g	29.7	24.4	67.6	62.5	32.6	22.4		34.4	46.5

^aEdge-to-edge distance measured between the 13-carbons (to which the linker is attached) of the two chlorins (see Charts 1 and 2). ^bDefined in Figure 5. ^cΔLUMO = E(LUMO^h) – (LUMO^l). ^dΔHOMO = E(HOMO^h) – (HOMO^l). ^eΔMO = (ΔLUMO + ΔHOMO)/2. ^fFor **C2-βAC** and **C2-βBTD**, the splitting is between the two MOs of the dyad that are highest and lowest energy of the three that result from mixing the MOs of the two chlorins and the linker, which are comparable energy in these cases. ^gDifference in energy of the Q_{1β} – Q_{1α} (split nominal Q_y) absorption bands (Figure 1 and Table 1). ^hFictive dyad **C2-βP0^h** lacks the alkoxy-like substituents on the phenyl group of the linker present in dyad **C2-βP** (Chart 2).

Table 5. MO energies for chlorin monomers and linkers.

	LUMO+1	LUMO	HOMO	HOMO-1
<i>Chlorin</i>				
C-βEm	-1.72	-2.31	-4.89	-5.04
C-βB	-1.73	-2.34	-4.86	-5.07
C-βV	-1.70	-2.33	-4.80	-5.04
C-βP	-1.72	-2.31	-4.89	-5.04
C-βAC	-1.72	-2.31	-4.89	-5.04
C-βBTD	-1.72	-2.31	-4.89	-5.04
<i>Linker</i>				
E		+1.43	-7.63	
B		+0.68	-10.37	
V		+0.51	-7.25	
P		-1.85	-5.88	
P0 ^a		-1.46	-5.90	
AC		-2.21	-5.12	
BTD		-2.66	-5.89	

^aThis linker for fictive dyad **C2-βP0** lacks the alkoxy-like substituents on the phenyl group of the linker used in dyad **C2-βP** (Chart 2).

Linker-mediated electronic communication between chlorins in a dyad depends on a number of factors. These factors include (1) the edge-to-edge distance between chlorins (Table 4), (2) the relative orientation of the chlorins with respect to each other and with the linker (Figures S2–S4 and Table S2), (3) the electron density at 13-position at which the linker is attached for each of the four frontier MOs of the benchmark chlorin (Figures 3–8), (4) the relative energy of the HOMO of the linker and the HOMO and HOMO-1 of the benchmark chlorin, and similarly (5) the relative energy of the LUMO of the linker and the LUMO and LUMO+1 of the benchmark chlorin (Figures 3–8 and Table 5). The relative energies of the analogous MOs of the linker and the chlorin contribute, along with spatial orbital overlaps (electronic coupling factors) to the mixing between the chlorin and linker MOs – orbitals closer together in energy give rise to greater mixing for the same spatial overlap. The relative magnitudes of the contributions of these factors likely underpin differences in the MO characteristics of the chlorin dyads depending on the nature of the linker, including the absence or presence and type of aromatic group in the linker (Chart 2).

Typically, the HOMO of chlorins is an $a_{1u}(\pi)$ -like orbital (D_{4h} symmetry designation), which places considerably more electron density at the β -pyrrole sites than at the *meso*-carbons, while the HOMO-1 is an $a_{2u}(\pi)$ -like orbital, which has the reverse relative electron densities at the two positions. The $e_{gx}(\pi^*)$ -like LUMO has significantly more electron density at the β -pyrrole 13-position of linker attachment (as well as at the 2, 3, and 12-positions) than at the β -pyrrole 7, 8, 17, 18-positions. The reverse is true for the symmetry related $e_{gy}(\pi^*)$ -like LUMO+1 (see e.g., Figure 6). Thus, one expects much greater interaction of the HOMO of the linker with the HOMO of the chlorin than with the HOMO-1 of the chlorin. Similarly, one

expects much greater interaction of the LUMO of the linker with the LUMO of the chlorin than with the LUMO+1 of the chlorin.

These effects are manifest in the MO diagram for the ethyne-linked dyad **C₂-βEm** (Figure 3). As expected, this dyad has characteristics very similar to analog **C₂-βE** studied previously [38], because the two differ only in having a mesityl vs tolyl group at non-linking 10-position (Chart 2 versus Chart 1). The HOMO-1^l (-5.08 eV) and HOMO-1^h (-5.12 eV) of dyad **C₂-βEm** differ very little in energy from each other and from HOMO-1 (-5.07 eV) of monomer **C₂-βEm**. Similarly, the LUMO+1^l (-1.74 eV) and LUMO+1^h (-1.74 eV) of dyad **C₂-βEm** are degenerate and have about the same energy as the LUMO+1 (-1.73 eV) of the parent chlorin. On the other hand, strong linker-mediated interaction between the HOMO of each chlorin gives rise to a pair of orbitals for **C₂-βEm**, the HOMO^l (-5.02 eV) and HOMO^h (-4.73 eV) split by 0.29 eV (Figure 3 and Table 4). Similarly, the LUMO^l (-2.48 eV) and LUMO^h (-2.16 eV) are linear combinations of the LUMOs of the chlorin constituents separated by 0.32 eV.

A similar MO pattern is observed for butadiyne-linked dyad **C₂-βBm** (Figure 4), except that the HOMO^l/HOMO^h splitting (0.26 eV) and LUMO^l/LUMO^h splitting (0.27) are both slightly smaller compared to those for **C₂-βEm**. The vinyl linker in **C₂-βV** affords much stronger interactions, giving rise to HOMO^l/HOMO^h and LUMO^l/LUMO^h splittings (0.33 and 0.35 eV) that are larger than those for **C₂-βEm** (0.29 and 0.32 eV) and **C₂-βBm** (0.26 and 0.27 eV). The HOMO and LUMO splittings thus increase as the distance between chlorins in the dyads decrease along the order **C₂-βBm** (~6.6 Å) > **C₂-βEm** (~4.0 Å) > **C₂-βV** (~3.8 Å) (Table 4).

Inspection of Figures 3–8 shows that the frontier MOs of the chlorins benchmarks and dyads are on the range -5.9 to -1.7 eV. The frontier MOs of the vinyl, ethynyl, and butadiynyl linkers of dyads **C₂-βV**, **C₂-βE**, and **C₂-βB** are far outside this window (Table 5). The HOMOs

of these three linkers have more negative energies (-7.2 to -10.4 eV) and the LUMOs have positive energies ($+0.50$ to $+1.4$ eV). On the other hand, the frontier MOs of the alkoxy-phenyl, anthracyl, and benzothiadiazole moieties of dyads **C₂- β P**, **C₂- β AC**, and **C₂- β BTd** are within the energy window of the chlorin MOs (Figures 6–8 and Table 5). The distances between chlorins in these three dyads are comparable to one another (~ 10.9 Å) and greater than for **C₂- β Bm** (~ 6.6 Å) by the placement of an aromatic group between the two ethynyl groups of abutadiynyl linker (Chart 2). Thus, differences in the MO characteristics among the three dyads that contain an aromatic group in the linker (**C₂- β P**, **C₂- β AC**, and **C₂- β BTd**) shown in Figures 6–8 must derive primarily from (1) moderate differences in the relative energies of the frontier MOs of the linker and chlorins and (2) differences in spatial relationships of the chlorins and the linker. The MO properties of these three dyads are described in the following.

C₂- β P reveals a slightly smaller HOMO^l/HOMO^h splitting (0.24 eV) than that for **C₂- β Bm** (0.26 eV; Table 4). The LUMO^l/LUMO^h splitting for **C₂- β P** (0.26 eV) is comparable to that for **C₂- β Bm** (0.27 eV). Thus, the presence of the substituted-phenyl ring appears to largely compensate for the ~ 4.3 Å larger distance between chlorins compared to its absence in the butadiynyl linker. Unlike **C₂- β Bm** (Figure 4), the degeneracy of the two MOs of **C₂- β P** originating from the monomer HOMO-1 is broken and the same is true for the two orbitals of the dyad originating from the LUMO+1 of the monomer (Figure 6). The splittings (0.21 and 0.20 eV, respectively) are somewhat smaller than the splittings for the above-noted orbitals of **C₂- β P** derived from the monomer HOMO and LUMO (0.24 and 0.26 eV). Furthermore, these HOMO-1^l/HOMO-1^h and LUMO+1^l/LUMO+1^h pairs show far less (if any) electron density on the phenyl ring of the linker, unlike the HOMO^l/HOMO^h and LUMO^l/LUMO^h pairs. This observation suggests that the splitting in the HOMO-1^l/HOMO-1^h and LUMO+1^l/LUMO+1^h pairs may not reflect a substantial contribution to electronic communication between chlorins.

Along these lines, calculations on fictive **C₂-βP0** that lacks the long alkoxy-like substituents on the phenyl ring of the linker shows a degenerate HOMO-1^l/HOMO-1^h pair and a degenerate LUMO+1^l/LUMO+1^h pair (Figure S7) rather than the split HOMO-1^l/HOMO-1^h pair and split LUMO+1^l/LUMO+1^h pair of **C₂-βP** (Figure 6). Furthermore, the splittings for HOMO^l/HOMO^h (0.16 eV) and LUMO^l/LUMO^h (0.17 eV) for **C₂-βP0** are reduced from those for **C₂-βP** (0.24 and 0.26 eV). These observations suggest that part of the HOMO^l/HOMO^h and LUMO^l/LUMO^h splittings and all of the HOMO-1^l/HOMO-1^h and LUMO+1^l/LUMO+1^h splittings for **C₂-βP** derive from steric interactions involving the alkoxy-like groups of the linker and substituents on the chlorin, and not from enhanced linker-mediated electronic communication between the chlorins. Dyad **C₂-βP** also shows a filled orbital (HOMO-4) at -5.85 eV that has electron density primarily (but not exclusively) on the linker. This dyad MO has comparable energy to the HOMO of the linker (-5.88 eV). Similarly, the dyad has an empty orbital (LUMO+4) at -1.58 eV that has substantial electron density on the linker (as well as some on the chlorins). That dyad MO has moderately higher energy than the LUMO of the linker (-1.85 eV) (Figure 6).

The energy gaps between the LUMO and HOMO of monomer **C-βAC** versus the **AC** linker (0.10 and 0.23 eV) are the smallest values of all the dyads (Table 5). The energy gap between the LUMO of **C-βBTD** versus **BTD** (0.35) is the next smallest value. The energy gap between the HOMO of **C-βBTD** versus **BTD** is somewhat larger (1.0 eV).

The characteristic that the MO diagrams for **C-βAC** and **C-βBTD** (Figures 7 and 8) have features in common with those for **C₂-βBm**, **C₂-βEm** and **C₂-βV** (Figure 3–5). In particular, the dyad MOs derived from the monomer HOMO-1 are essentially a degenerate pair and the same is true for the pair of dyad MOs originating from the monomer LUMO+2. These orbitals are identified in the figures by the use of blue font for the orbital energies. Again, this finding is

expected because the monomer HOMO-1 and LUMO+1 have do not have substantial electron density at the chlorin β -pyrrole 13-position of linker attachment. In contrast, because of good orbital overlap and relatively close MO energies, there is substantial mixing among the HOMO of the two chlorins and the HOMO of the linker for the **C2- β AC** and **C2-BBTD** dyads. Similarly, substantial mixing occurs among the LUMOs of the two chlorins and the LUMO of the linker for these dyads.

The above results for the dyads containing the aromatic linker show that sets of three HOMO-derived MOs and three LUMO-derived MOs (Figures 7 and 8) are generated instead of the split pairs arising for the dyads lacking the aromatic unit in the linker (Figure 4–6). Extending the convention noted in Figure 9 and used above for dyads for **C2- β B**, **C2- β E** and **C2- β V** three filled orbitals of for **C2- β AC** and **C2- β BTD** are denoted HOMO^l, HOMO^m and HOMO^h, where the superscripts l, m, and h refer to lowest, middle, and highest in energy. Similarly, the trio of empty orbitals of the latter two dyads are denoted LUMO^l, LUMO^m and LUMO^h. The generation of three orbitals for the dyad is analogous to combining an orbital on one atom (e.g., 1s) with two orbitals on another atom (e.g., 2p_x and 2p_y) to generate bonding, nonbonding and antibonding MOs from lower to higher energy. The nonbonding MO has effectively no electron density between constituents and typically has an energy the same as or close to that of one of the constituent atomic orbitals. Examination of Figures 7 and 8 for the HOMO^l/HOMO^m/HOMO^h trio and the LUMO^l/LUMO^m/LUMO^h trio (MO energies in red font) shows that the middle orbital in each set has these characteristics of a nominal nonbonding MO. There is no electron density on the aromatic ring (but some on the ethynyl groups), and the orbital is close in energy to the HOMO or LUMO of the parent chlorin. In particular, the LUMO^m of **C2- β AC** or **C2- β BTD** (–2.32 or –2.31 eV) has basically the same energy as the

LUMO of the chlorin monomer (−2.31 eV) and the HOMO^m of **C₂-βAC** or **C₂-βBTD** (−4.99 eV) has slightly lower energy than the HOMO chlorin monomer (−4.89 eV).

On the other hand, the highest and lowest energy MOs of the trios (HOMO^h/HOMO^l and LUMO^h/LUMO^l) have electron density delocalized across the **C₂-βAC** and **C₂-βBTD** dyads including the linker (Figures 7 and 8). Furthermore, the splitting for HOMO^h/HOMO^l and LUMO^h/LUMO^l is greater for **C₂-βAC** (0.61 and 0.63 eV) and **C₂-βBTD** (0.88 and 0.58 eV) than for the pairs of MOs in dyad **C₂-βBm** that lacks the aromatic group between the two ethynes of the (butadiynyl) linker (0.26 eV and 0.27 eV) (Table 4). The HOMO^h/HOMO^l and LUMO^h/LUMO^l splittings for **C₂-βAC** (0.61 and 0.63 eV; average 0.63) versus **C₂-βBTD** (0.88 and 0.58 eV; average 0.73) should not be taken alone to gauge the relative extents of electron delocalization and electronic communication between the two chlorins in the dyads. The relative energies of the contributing MOs and the shapes of the electron densities in the dyad MOs play a role. As noted above, the energy difference between HOMO/LUMO of chlorin monomer and the HOMO/LUMO of the linker is smaller for **C₂-βAC** (0.10/0.23) than **C₂-βBTD** (0.35/1.0) (Table 5). Hence, other (structural) factors being equal, greater MO mixing might be expected for **C₂-βAC** than **C₂-BTD**. In this regard, the frontier MOs closest to HOMO and LUMO of chlorin monomer have larger shift in energy for **C₂-βAC** (0.21/0.27 for HOMO^l/LUMO^h) than those for **C₂-βBTD** (0.1/0.1 for HOMO^l/LUMO^h), indicating the greater MO mixing for **C₂-Bac** (Figure 7 and Table 5). However, HOMO^l (−5.67 eV) and LUMO^l (−2.79 eV) **C₂-βBTD**, the frontier MOs closest in energy to the HOMO (−5.89 eV) and LUMO (−2.66 eV) of **BTD** linker have the greatest electron density on the linker (Figure 8). The extent of MO mixing depending on energy difference and electronic interactions between a tetrapyrrole and a conjugated linker has been reported previously in a study of *meso*-linked porphyrin dyads [21]. Regardless of the

balance of such structural and energetic factors, the presence of the anthracenyl or benzothiadiazole group in the linker more than compensates for the increased distance between the two chlorins and adds an additional element to enhance electronic communication.

IV. DISCUSSION

A. Ground-State Properties. The β -linked chlorin dyads studied here reveal photophysical, redox, and MO characteristics that differ from the corresponding benchmarks due to strong electronic interactions between the constituent macrocycles. The new dyads that employ ethynyl and butadiynyl linkers have properties similar to analogs studied previously [38]. A dyad with a vinyl linker extends this series. The new dyads that contain an aromatic unit (substituted phenyl, anthracyl or benzothiadiazole) between two ethynyl groups have properties distinct from one another and the other dyads due to more extensive mixing involving the MOs of the linker and the chlorin macrocycles. Compared to the ethynyl- and butadiynyl-linked chlorins, the other new dyads, when referenced to the corresponding benchmarks, exhibit (1) intermediate bathochromic shifts and splittings of the lowest-energy (Q_y -derived) absorption band in the far red region, (2) substantial changes in excited-state properties that are generally favorable for most applications (except for quenching in a polar medium in one case), and (4) redox potentials that are generally similar to the benchmarks albeit associated with split redox waves.

The significant electronic communication between chlorins in the new dyads are manifested by two key ground-state properties. One is split redox waves (Table 3). The other is that the dyads contain (1) pairs of MOs that are linear combinations of the MOs of the constituent chlorins, or (2) and trios of MOs that additionally involve substantial mixing with the

anthracyl and benzothiazole units of the linkers of **CAC** or **C₂- β BTB** (Figures 3-8). The observation of linear-combination MOs is consistent with previous theoretical predictions for tetrapyrrolic dyads bearing conjugating linkers [49]. Furthermore, calculations performed on fictive version of dyads in the linker is removed but the spatial relationship between chlorin constituents remains unchanged demonstrates that the interactions between chlorins are mediated by the linker with little if any through-space character (Figures S5 and S6). As we have noted previously [38], such substantial changes in ground-state characteristics compared to those of the chlorin monomers precludes the use of a standard exciton model to describe the optical properties of these dyads. The standard exciton model is based on the coupling of excited-state transition dipoles and assumes no significant ground-state interactions [46,51]. Rather, as described above and further below, such observations can be qualitatively understood in terms of the effects of strong electronic interactions of the MOs of the constituents.

Torsional motions involving the relative orientations of the two chlorins with respect to the linker (and each other) likely contribute substantially to the properties of the dyads. The DFT calculations reported here (Figure S2) and previously [38,49] indicate that the torsional potential energy surface for rotation about an ethynyl or butadiynyl linker is relatively broad in the vicinity of the global and local minima, has barriers that are relatively small (<1.5 kcal/mol) and a maximum in the vicinity of 90° where electronic communication via the linker is absent. As we have noted previously [38], a rigorous model for the effects of torsional motion on the electronic properties of the dyads would require inclusion of the full vibrational manifold for the low-frequency, anharmonic torsional motion on both the ground and excited electronic state potential surfaces. Furthermore, the ‘conformational space’ accessed by the dyad at a given temperature reflects the Boltzmann populations of the thermally accessible sublevels of the torsional modes. For simplicity, we have used a static description of the electronic interactions

in the dyads in terms of linear combinations of constituent MOs to qualitatively describe the trends in optical properties of the dyads with the nature of the conjugated linker.

The optical spectra of tetrapyrroles are often described in terms of Gouterman's four-orbital model [4–6]. Within this model, the B_y , B_x , Q_x , and Q_y bands that span the near-UV to NIR regions are associated with excited states derived from binary combinations of the four one-electron configurations involving electron promotions involving the HOMO-1, HOMO, LUMO and LUMO+1. Direct application of this model to optical spectra of the chlorin dyads would be an oversimplification. However, the spectra of the dyads have features in the same general spectral regions as the monomers, albeit shifted and split in many instances. Thus, it is convenient to use the model depicted in Figure 9 involving pairs of dyad MOs originating from the related four-orbital-model MOs of the monomers as a general framework to describe the key aspects of the spectra. Figure 9 shows 8 of the 16 possible one-electron promotions between dyad orbitals that are optically allowed if the two macrocycles of the dyad are in the coplanar *anti*-configuration (C_{2h} symmetry). Dyads **C2-βBm**, **C2-βEm**, **C2-βV**, and **C2-βP**, whose spectra are shown in Figures 3–6, are shown in Figure 9, have an *anti*-conformation. All 16 of the one-electron promotions are allowed if a dyad assumes the coplanar *syn*-configuration which is the preferential configuration for **C2-βAC** and **C2-βBTD**. Thus, for dyads that have the *anti*-configuration lowest, torsional motions that access internal torsional angles away from 180° will lead to broadening or doubling of the bands in the absorption spectra.

The illustration in Figure 9 shows four pairs of one-electron promotions involving dyad HOMO^l and HOMO^h that are split from the monomer HOMO and involving the dyad LUMO^l and LUMO^h that are split from the monomer LUMO. Such pairs of dyad MOs is appropriate for **C2-βBm**, **C2-βEm**, **C2-βV**, and **C2-βP** (Figures 3–6). Specific linear combinations of the one-

electron promotions for the dyad leads to split levels in the excited-state manifold and to spectrally split $Q_{1\beta}$ and $Q_{1\alpha}$ bands, which are related to the monomer Q_y band. For dyads **C2- β AC** and **C2- β BTd**, the $HOMO^l$ and $HOMO^h$ sandwich a third orbital $HOMO^m$ that has no electron density on the aromatic unit of the linker, and there is an analogous trio of empty orbitals in which $LUMO^m$ lies intermediate in energy between $LUMO^l$ and $LUMO^h$ (Figures 7 and 9). Again, specific linear combination of the one-electron promotions involving split $HOMO^l/HOMO^h$ and $LUMO^l/LUMO^h$ of **C2- β AC** and **C2- β BTd** would give split levels in the excited-state manifold and the split $Q_{1\beta}$ and $Q_{1\alpha}$ bands.

A notable feature of the electronic structure of the chlorin dyads is the varied splitting of the $HOMO^l/HOMO^h$ and $LUMO^l/LUMO^h$ derived from the HOMO and LUMO of the chlorins, and the HOMO and LUMO of the linker depending on the dyad (Figures 3-8 and Table 4). A related notable characteristic of the absorption spectra of the dyads that employ different conjugated linkers is the different magnitude of the band splitting ($Q_{1\beta}/Q_{1\alpha}$) in the lowest absorption band (Tables 1 and 4). The linkers vary in length (Table 4) and the energies and electron densities of their MOs (Figures 3-8 and Table 5). Figure 10 makes pairwise comparisons of several of these MO and spectral characteristics to help visualize differences among the dyads. The points in blue are for dyads **C2- β Em**, **C2- β E**, **C2- β Bm**, **C2- β B**, and **C2- β V**, which do not an aromatic unit in the linker and the points labeled red are for dyads **C2- β P**, **C2- β Bm**, and **C2- β Bm**, which contain an aromatic ring between the two ethynyl groups of the linker.

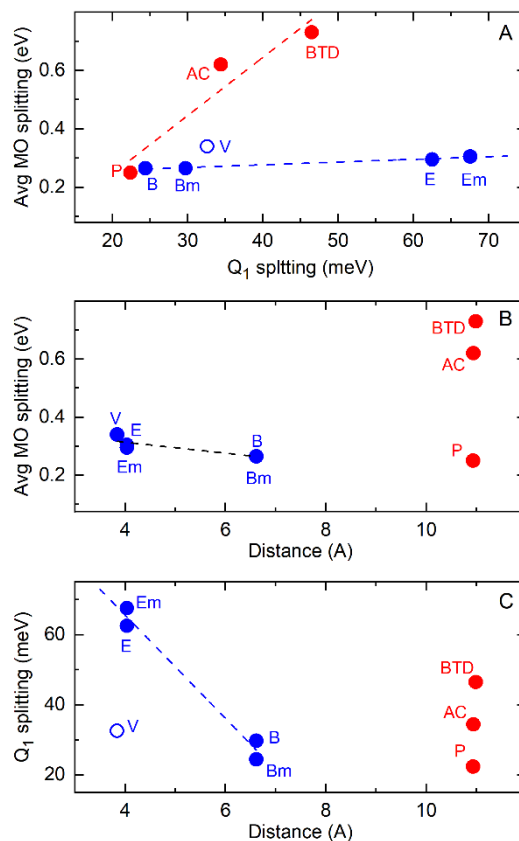


Figure 12. Comparison of properties of dyads (Charts 1 and 2) that employ (red) an ethynyl (E or Em), butadiynyl (B or Bm) or vinyl (V) linker or (blue) an alkoxyphenyl (P), anthracyl (AC) or benzothiadiazole (BTD) linker. (A) Average of HOMO and LUMO splittings versus splitting of the $Q_{1\beta}$ and $Q_{1\alpha}$ (e.g., Q_y) absorption bands. (B) Average of HOMO and LUMO splittings versus edge-to-edge distance between chlorins. (C) Splitting of the $Q_{1\beta}$ and $Q_{1\alpha}$ (e.g., Q_y) absorption bands versus edge-to-edge distance between chlorins. The colored dashed lines are fits to the data points of the same color, except for panels A and C where the point for the vinyl-linked dyad was not included in the fits (see text).

The HOMO^l/HOMO^h and the LUMO^l/LUMO^h splittings for **C₂-βEm** (0.29 and 0.32 eV) and **C₂-βBm** (0.26 and 0.27 eV) are similar to those observed previously²⁸ for analogs **C₂-βE** (0.29 and 0.30 eV) and **C₂-βE** (0.27 and 0.26 eV) and provide useful reference points for the other dyads. The roughly two-fold greater $Q_{1\beta} - Q_{1\alpha}$ splitting for **C₂-βEm** (~68 mV) and **C₂-βBm** (~30 meV) reflects the shorter edge-to-edge distance for **C₂-βEm** (~4.0 Å) than **C₂-βBm** (~6.6 Å). The vinyl linker in **C₂-βV** affords the shortest distance between chlorins (~3.8 Å) and HOMO^l/HOMO^h and the LUMO^l/LUMO^h splittings (0.33 and 0.35 eV) that are larger than those

for both **C₂-βEm** and **C₂-βm** (Table 4 and blue points in Figure 10B). The vinyl linker also provides a rigid structure with a large barrier to internal rotations (Figure S2C). On the other hand the apparent $Q_{1\beta} - Q_{1\alpha}$ spectral splitting (~33 meV) for **C₂-βV** is intermediate in magnitude and closer to that for **C₂-βm** (Table 4 and blue points in Figure 3C). The reason for the latter dichotomy is not clear at present. One possibility is uncertainty in estimating the wavelength of the $Q_{1\beta}$ feature for **C₂-βV** (Figure 1F, red) within the broad contour to shorter wavelengths than the 710 nm peak ($Q_{1\beta}$) that extends to ~770 nm along with a weak feature at ~650 nm. [Note that such a broad tail extends from the ~700 nm maximum to below 600 nm for zinc chelate **ZnC₂-βV** (Figure 1F, green).] The $Q_{1\beta}$ band along with vibronic overtones or features derived from other torsional configurations could all contribute to the contour. If $Q_{1\beta}$ lies at 683 nm rather than 697 initially estimated (from Gaussian fitting), then the spectral splitting would increase to 70 meV and fall on the blue dashed lines in Figures 10A and 10C derived from the data for **C₂-βm** and **C₂-βm**.

Dyads **C₂-βP**, **C₂-βAC** and **C₂-βBTD** all have an aromatic group between the two ethyne groups of the butadiynyl linker of **C₂-βBm**, which then serves as a reference point. The aromatic group increases the edge-to-edge distance between chlorins (Table 5) by essentially the same amount for **C₂-βBTD**, **C₂-βP**, and **C₂-βAC** (~10.9 Å) compared to **C₂-βBm** (~6.6 Å). The added linker length which would tend to reduce electronic communication between chlorins for the former three dyads compared to the latter. The HOMO^l/HOMO^h and LUMO^l/LUMO^h splittings on the average increase in the order **C₂-βP** (0.24 and 0.26 eV) < **C₂-βBm** (0.26, 0.27 eV) < **C₂-βAC** (0.61 and 0.63 eV) < **C₂-βBTD** (0.88 and 0.58 eV) (Table 4). The $Q_{1\beta} - Q_{1\alpha}$ spectral splitting (Tables 1 and 4) increases in the order **C₂-βP** (22.4 meV; 180 cm⁻¹) < **C₂-βBm** (29.7 meV; 240 cm⁻¹) < **C₂-βAC** (34.4 meV; 277 cm⁻¹) < **C₂-βBTD** (46.5 meV; 375 cm⁻¹). The

connection between these two parameters for the three dyads containing an aromatic unit in the linker is given by the red line in Figure 10A. The results suggest that the alkoxy-phenyl group of **C2- β P** almost counterbalances the increased distance from to **C2- β Bm** and that the anthracyl group of **C2- β AC** and the benzodiathiazole group of **C2- β BTd** more than compensate and increases the net electronic communication between chlorins compared to the butadiynyl linker. The collective findings indicate that the electronic characteristics of the conjugated linker between chromophores impacts the electronic structure of the dyads as much if not more than the inter-chromophore distance. This finding is consistent with the results of prior studies of porphyrin dyads that contain various conjugated linkers [21].

B. Excited-State Properties. The rate constant k_f for $S_1 \rightarrow S_0$ spontaneous fluorescence is obtained from the measured fluorescence yield and singlet excited state lifetime ($k_f = \Phi_f \div \tau_S$). The values in Table 1 show that k_f increases on the average about two-fold from $\sim(20 \text{ ns})^{-1}$ for the chlorin monomers to $\sim(9.3 \text{ ns})^{-1}$ for the chlorin dyads. The increased k_f is expected to be accompanied by a parallel increase in the probability for $S_0 \rightarrow S_1$ absorption via the relationships of the Einstein coefficients and Strickler-Berg implementation for molecular systems [46]. The absorption spectra shown in Figure 1 for the chlorin monomers and dyads in toluene are normalized to the same total integrated intensity to facilitate comparisons. On a per-molecule basis, one would expect double the total intensity for the dyad versus the monomer. The $S_0 \rightarrow S_1$ absorption transition corresponds to the Q_y band of the monomer and the $Q_{1\alpha}$ band of the dyad, along with associated vibronic overtone features. The $Q_{1\beta}$ band of the dyads corresponds to the $S_0 \rightarrow S_2$ transition. If Q_y intensity for a monomer were split equally between the $Q_{1\beta}$ and $Q_{1\alpha}$ bands of the dimer, then one might have expected the $S_0 \rightarrow S_1$ radiative rate constant, and the associated k_f for $S_1 \rightarrow S_0$ to be about the same for the dyad and monomer. However, differences

in the overlaps (signs and electron densities) of the MOs involved along with differences in configurational mixing apparently contribute to greater (roughly and perhaps fortuitously double) intensity in the $S_0 \rightarrow S_1$ ($Q_{1\alpha}$) versus $S_0 \rightarrow S_2$ ($Q_{1\beta}$) transitions of the dyad.

Relevant here is the observation from Figure 1 that the integrated violet-blue Soret absorption manifold of a given dyad is generally lower than that for the corresponding monomer. This difference could be associated with increased intensity in the $Q_{1\alpha}$ (and perhaps $Q_{1\beta}$) features for the dyad. Recall also that the $Q_{1\alpha}$ band of the dyads is bathochromically shifted by 30 nm on the average from the Q_y band of the monomers, and appears to be associated with both splitting ($\Delta\lambda_{Q1}^{\text{split}}$) of the $Q_{1\beta}/Q_{1\alpha}$ bands and a shift ($\Delta\lambda_{Q1}^{\text{shift}}$) in center-of-gravity of $Q_{1\beta}$ and $Q_{1\alpha}$ for a dyad versus Q_y for the monomer (Figure 1 and Table 1). In fact, hyperchromic/bathochromic effects on the intensity/wavelength of the Q_y absorption correlated with hypochromic/hypsochromic effects on the intensity/wavelength of the B_y (a component of Soret) absorption of tetrapyrroles is an integral aspect of the four-orbital model [4–6]. Such intensity/spectral effects on the Q_y and B_y transitions is associated with changes in the coefficients describing the destructive/constructive interference in admixtures of the excited-state configurations derived from the one-electron promotions depicted in Figure 9.

Under the four-orbital model, changes in configurational mixing could arise from a change in MO energy gaps (the energy denominator in the mixing formula) or in the configuration-interaction energy (the numerator in the mixing formula). The MO energies (and energy gaps) have clearly changed in the dyads versus the monomers (Figures 3–8 and Tables 4 and 5). However, the configuration-interaction energy is also likely reduced in a strongly-coupled dyad versus the constituent monomers. Delocalization of electron density throughout the dyad implies that one chlorin effectively increases the size of the electron box for the second

chlorin, and vice versa. This delocalization will reduce the configuration interaction energy, decrease mixing of the relevant excited-state configurations in the four-orbital model, and shift intensity from B_y (Soret) to Q_y (or $Q_{1\alpha}/Q_{1\beta}$). This intensity redistribution is typically accompanied by a bathochromic shift in the Q_y state, which is associated with the long wavelength absorption band. A similar effect of reduced configuration interaction energy associated with electron delocalization has been noted concerning the panchromatic absorption displayed by porphyrins, chlorins and bacteriochlorins strongly coupled to a chromophore such as a perylene monoimide [52–54]. Thus, a reduced configuration-interaction in addition to altered MO energetics both may make significant contributions to the spectral properties of the strongly coupled chlorin dyads, including increased $S_0 \leftrightarrow S_1$ radiative probabilities (and k_f).

An increased k_f in a dyad versus the benchmark monomer will necessarily increase the fluorescence yield, all other factors being the same. The average Φ_f value of the dyads (0.56) is indeed larger than that for the monomers (0.42) in both toluene (Table 1) and benzonitrile (Table S1). That $\Phi_f = k_f / (k_f + k_{isc} + k_{ic}) = k_f \times \tau_S$ does not increase roughly two-fold (along with k_f) in the dyads versus monomers is because the rate constant for internal conversion (k_{ic}) generally increases in the dyad versus monomer (in either solvent) as well (Tables 1 and S1). The greater k_f and k_{ic} (and relatively unchanged k_{isc}) in the dyads versus the monomers contribute to the average smaller τ_S in the dyads (5.2 ns) than the monomers (8.2 ns) (Tables 1 and S1).

More facile $S_0 \rightarrow S_1$ internal conversion in the dyads versus the monomers occurs for two reasons. The lower S_1 energy of in the dyads ($Q_{1\alpha}$) versus the monomers (Q_y) will enhance internal conversion via the energy-gap law for non-radiative decay [46]. Furthermore, internal conversion can be facilitated by molecular motions that alter disposition of the two chlorins with

respect to each other and thus the admixture of four basis configurations (A^*A , AA^* , A^-A^+ and A^+A^-) that define the electronic character of the S_1 state.

Comparison of Tables 1 and S1 show that all the dyads except **C2- β BTD** show a moderate factor of 1.1–1.7 reduction in singlet excited-state lifetime and fluorescence yield for the molecules in benzonitrile versus toluene. These differences reflect a small factor of 1.2–2.7 increase in the rate constant for internal conversion in the more polar solvent. In comparison, for **C2- β BTD** τ_s is reduced by a factor of 3.4 and Φ_f by a factor of 3.7, both derived from a 26-fold increase in k_{ic} in the more polar solvent. Typically, excited-state quenching in a polar medium is described by the involvement of a charge-transfer (CT) state that is stabilized in the polar medium and drops below the lowest (neutral) excited state and provides a new pathway for non-radiative deactivation. However, for the strongly coupled dyads, in the absence of perturbations such as transient solvent symmetry breaking, the two CT configurations have equal energy, and linear combinations give charge resonance (CR) configurations ($A^+A^- \pm A^-A^+$). Similarly, the two locally-excited configurations have equal energy and admixtures produce ‘exciton’ configurations ($A^*A \pm AA^*$). Typically, the S_1 excited state of such a dyad in nonpolar media will be dominated by one of the exciton configurations, with little admixture of a (higher energy) CR configuration.

Coulomb stabilization of ($A^+A^- \pm A^-A^+$) in a polar medium will increase the contribution along with ($A^*A \pm AA^*$) to the nature of S_1 state, making the state more polarizable (but not more polar). If the solvent stabilization is significant enough the new lowest excited state of the dyad will have primarily CR character, but still no net CT character unless transient structural or solvent motions break the symmetry. Such increased CR contributions to the electronic character of S_1 likely accounts for the moderate enhancement of internal conversion for the

dyads in benzonitrile versus toluene. Increased CR character could also contribute to larger enhancement of internal conversion for **ZnC₂-βV** in benzonitrile versus toluene, compared to the enhancement observed for **C₂-βV**. Larger charge-resonance character is thought to account for the more pronounced solvent-polarity dependence of the lowest excited state of strongly coupled bacteriochlorin dyads compared to the chlorin counterparts and zinc chelates versus corresponding free base dyads [38,55].

The much greater enhancement for **C₂-βBTD** compared to the other dyads studied here could be associated with the additional contribution of electronic configurations such as ($A^+L^-A \pm AL^-A^+$) or ($AL^+A^- \pm A^-L^+A$) involving charge transfer between the chlorins and the BDT unit of the linker (L). One such configuration could be at sufficiently low energy to contribute substantially to the properties of S_1 due to the relatively close proximity of the frontier MOs of the linker and the chlorins (Figure 8). Motions that make the interactions involving the BTD unit and one chlorin different than with the other chlorin could introduce net CT character and further enhance non-radiative deactivation of **C₂-βBTD** in the polar medium. Except for **C₂-βBTD** the photophysical properties of the lowest excited state of the other dyads are not particularly solvent dependent and are favorable for use in a number of applications.

In conclusion, relative to the benchmark monomers, the β-linked chlorin dyads studied herein have significantly altered spectral, excited-state and molecular-orbital derived strong linker-mediated electronic communication between the chlorin. The comprehensive study of the effects of linkers on chlorin dyads will augment design strategies for new light-harvesting arrays for solar-energy conversion and fluorescent probes for NIR imaging.

ASSOCIATED CONTENT

Supporting Information

Synthesis methods and chemical characterization data; tabulated spectral characteristics of the dyads and benchmarks in benzonitrile; absorption and fluorescence emission spectra of dyads and benchmarks in benzonitrile; analysis of the torsional motions in the dyads. This material is available free of charge via the Internet at <http://pubs.acs.org>.

AUTHOR INFORMATION

Corresponding Authors

*E-mail: mptaszek@umbc.edu (M.P.); holten@wustl.edu (D.H.); david.bocian@ucr.edu (D.F.B.).

Notes

The authors declare no competing financial interest.

ACKNOWLEDGEMENTS

Work at WU and UCR was supported by the Division of Chemical Sciences, Geosciences, and Biosciences, Office of Basic Energy Sciences of the U.S. Department of Energy grant DE-FG02-05ER15661 (to D.H. and D.F.B). Work at UMBC was supported by U. of Maryland, Baltimore County (start-up funds and SRAIS Award) and the National Science Foundation under CHE-1301109 (M.P.). We thank Mr. John Arthur and Shirag Pancholi for assistance in dyad synthesis. D.N.M. acknowledges Center for Solar Energy and Energy Storage at McKelvey School of Engineering at Washington University in Saint Louis for financial support.

REFERENCES

1. Gueymard CA. The Sun's Total and Spectral Irradiance for Solar Energy Applications and Solar Radiation Models. *Sol. Energy* 2004; **76**: 423–453.
2. Oertel M, Schastak SI, Tannapfel A, Hermann R, Sack U, Mossner J and Berr F. Novel bacteriochlorine for high tissue-penetration: photodynamic properties in human biliary tract cancer cells in vitro and in a mouse tumour model. *J. Photochem. Photobiol. B* 2003; **71**:1-10.
3. Agostinis P, Berg K, Cengel K A, Foster TH, Girotti AW, Gollnick SO, Hahn SM, Hamblin M R, Juzeniene A, Kessel D, Korbelik M, Moan J, Mroz P, Nowis D, Piette J, Wilson BC and Golab J. Photodynamic therapy of cancer: An update. *CA Cancer J. Clin.* 2011; **61**: 250–281.
4. Gouterman M. Optical Spectra and Electronic Structure of Porphyrins and Related Rings. In *The Porphyrins*; Dolphin, D., Ed.; Academic Press: New York, 1978; **Vol. 3**: pp 1–165.
5. Gouterman M. Study of the Effects of Substitution on the Absorption Spectra of Porphin. *J. Chem. Phys.* 1959; **30**: 1139–1161.
6. Gouterman M. Spectra of Porphyrins. *J. Mol. Spectroscopy* 1961; **6**: 138–163.
7. Scheer H. In *Chlorophylls*; Scheer, H., Ed.; CRC Press: Boca Raton, FL, 1991; pp 3-30.
8. Kee HL, Kirmaier C, Tang Q, Diers JR, Muthiah C, Taniguchi M, Laha JK, Ptaszek M, Lindsey JS, Bocian DF and Holten D. Effects of Substituents on Synthetic Analogs of Chlorophylls. Part 2: Redox Properties, Optical Spectra and Electronic Structure. *Photochem. Photobiol.* 2007; **83**: 1125–1143.
9. Yang E, Kirmaier C, Krayner M, Taniguchi M, Kim HJ, Diers JR, Bocian DF, Lindsey JS and Holten D. Photophysical Properties and Electronic Structure of Stable, Tunable Synthetic Bacteriochlorins: Extending the Features of Native Photosynthetic Pigments. *J. Phys. Chem. B* 2011; **115**: 10801–10816.
10. Faries KM; Diers JR, Springer JW, Yang E, Ptaszek M, Lahaye D, Krayner M, Taniguchi M, Kirmaier C, Lindsey JS, Bocian DF and Holten D. Photophysical properties and electronic structure of chlorin–imides: Bridging the gap between chlorins and bacteriochlorins. *J. Phys. Chem. B* 2015; **119**: 7503–7515.
11. Vairaprakash P, Yang E, Sahin T, Taniguchi M, Krayner M, Diers JR, Wang A, Niedzwiedzki DM, Kirmaier C, Lindsey JS, Bocian D and Holten D. Extending the Short and Long Wavelength Limits of Bacteriochlorin Near-infrared Absorption via Dioxo- and Bisimide-Functionalization. *J. Phys. Chem. B* 2015; **119**: 4382–4395.
12. Fujita H, Jing H, Krayner M, Allu S, Veeraraghavaiah G, Wu Z, Jiang J, Diers JR, Magdaong NCM, Mandal AK, Roy A, Niedzwiedzki DM, Kirmaier C, Bocian DF, Holten D and Lindsey JS. *Annulated Bacteriochlorins for Near-Infrared Photophysical Studies*, *New J. Chem.* **2019**, 3, 7209–7232.
13. Kim D and Osuka A. In *Multiporphyrin Arrays*; Kim, D. Ed; Pan Sanford Publishing Pte. Ltd: Singapore, 2012, pp 1–44.
14. Lin VSY, Dimagno SG and Therien MJ. Highly Conjugated, Acetylenyl Bridged Porphyrins: New Models for Light-Harvesting Antenna Systems. *Science* 1994; **264**: 1105–1111.
15. Lin VSY and Therien MJ. The Role of Porphyrin-to-Porphyrin Linkage Topology in the Extensive Modulation of the Absorptive and Emissive Properties of a Series of Ethynyl- and Butadiynyl-Bridged Bis- and Tris(porphinato)zinc Chromophores. *Chem. Eur. J.* 1995; **1**: 645–651.
16. Kumble R, Palese S, Lin VSY, Therien MJ and Hochstrasser RM. Ultrafast Dynamics of Highly Conjugated Porphyrin Arrays. *J. Am. Chem. Soc.* 1998; **120**: 11489–11498.

17. Shediach R, Gray MHB, Uyeda HT, Johnson RJ, Hupp JT, Angiolillo PJ and Therien MJ. Singlet and Triplet Excited States of Emissive, Conjugated Bis(porphyrin) Compounds Probed by Optical and EPR Spectroscopic Methods. *J. Am. Chem. Soc.* 2000; **122**: 7017–7033.
18. Duncan TV, Susumu K, Sinks LE and Therien MJ. Exceptional Near-Infrared Fluorescence Quantum Yields and Excited-State Absorptivity of Highly Conjugated Porphyrin Arrays. *J. Am. Chem. Soc.* 2006; **128**: 9000–9001.
19. Duncan TV, Wu SP and Therien MJ. Ethyne-Bridged (Porphinato)Zinc(II)-(Porphinato)Iron(III) Complexes: Phenomenological Dependence of Excited-State Dynamics upon (Porphinato)Iron Electronic Structure. *J. Am. Chem. Soc.* 2006; **128**: 10423–10435.
20. Duncan TV, Ishizuka T and Therien MJ. Molecular Engineering of Intensely Near-Infrared Absorbing Excited States in Highly Conjugated Oligo(porphinato)zinc-(Polypyridyl)metal(II) Supermolecules. *J. Am. Chem. Soc.* 2007; **129**: 9691–9703.
21. Susumu K, Duncan TV and Therien MJ. Potentiometric, Electronic Structural, and Ground- and Excited-State Optical Properties of Conjugated Bis[(Porphinato)zinc(II)] Compounds Featuring Proquinoidal Spacer Units. *J. Am. Chem. Soc.* 2005; **127**: 5186–5195.
22. Piet JJ, Warman JM and Anderson HL. Photo-induced Charge Separation on Conjugated Porphyrin Chains. *Chem. Phys. Lett.* 1997; **266**: 70–74.
23. Taylor PN, Wylie AP, Huuskonen J and Anderson HL. Enhanced Electronic Conjugation in Anthracene-Linked Porphyrins. *Angew. Chem. Int. Ed.* 1998; **37**: 986–989.
24. Piet JJ, Taylor PN, Anderson HL, Osuka A and Warman JM. Excitonic Interactions in the Singlet and Triplet Excited States of Covalently Linked Zinc Porphyrin Dimers. *J. Am. Chem. Soc.* 2000; **122**: 1749–1757.
25. Winters MU, Kärnbratt J, Eng M, Wilson CJ, Anderson HL and Albinsson B. Photophysics of a Butadiyne-Linked Porphyrin Dimers: Influence of Conformational Flexibility in the Ground and First Singlet Excited State. *J. Phys. Chem. C* 2007; **111**: 7192–7199.
26. Kuimova MK, Hoffmann M, Winters MU, Eng M, Balaz M, Clark IP, Collins HA, Tavender SM, Wilson CJ, Albinsson B, Anderson HL, Parker AW and Phillips D. Determination of the Triplet State Energies of a Series of Conjugated Porphyrin Oligomers. *Photochem. Photobiol. Sci.* 2007; **6**: 675–682.
27. Chang MH, Hoffmann M, Anderson HL and Herz LM. Dynamics of Excited-State Conformational Relaxation and Electronic Delocalization in Conjugated Porphyrin Oligomers. *J. Am. Chem. Soc.* 2008; **130**: 10171–10178.
28. Kocherzhenko AA, Patwardhan S, Grozema FC, Anderson HL and Siebbeles LDA. Mechanism of Charge Transport along Zinc Porphyrin-Based Molecular Wires. *J. Am. Chem. Soc.* 2009; **131**: 5522–5529.
29. Sedghi G, Esdalié LJ, Anderson HL, Martin S, Bethell D, Higgins SJ and Nichols RJ. Comparison of the Conductance of Three Types of Porphyrin-Based Molecular Wires: β , *meso*, β -Fused Tapes, *meso*-Butadiyne-Linked and Twisted *meso-meso* Linked Oligomers. *Adv. Mater.* 2012; **24**: 653–657.
30. Kelley RF, Lee SJ, Wilson TM, Nakamura Y, Tiede DM, Osuka A., Hupp JT and Wasielewski MR. Intramolecular Energy Transfer within Butadiyne-Linked Chlorophyll and Porphyrin Dimer-Faced, Self-Assembled Prisms. *J. Am. Chem. Soc.* 2008; **130**: 4277–4284.
31. Sasaki S, Mizutani K, Kunieda M and Tamiaki H. Synthesis and Optical Properties of C3-Ethynylated Chlorin and π -Extended Chlorophyll Dyads. *Tetrahedron* 2011; **67**: 6065–6072.

32. Jaquinod L, Nurco D, Medforth CJ, Pandey RK, Forsyth TP, Olmstead MM and Smith KM. Planar Bischlorophyll Derivatives with a Completely Conjugated π -System: Model Compounds for the Special Pair in Photosynthesis. *Angew. Chem. Int. Ed.* 1996; **35**: 1840–1842.
33. Li G, Dobhal MP, Graham A, Shibata M, Zheng G, Kozyrev A and Pandey RK. Thermolysis of *vic*-Dihydroxybacteriochlorins: Effect of the Nature of Substrates in Directing the Formation of Chlorin-Chlorin Dimers with Fixed and Flexible Orientations and Their Preliminary in Vitro Photosensitizing Efficacy. *J. Org. Chem.* 2003; **68**: 3762–3772.
34. Wasielewski MR. In Chlorophylls; Scheer, H., Ed.; CRC Press: Boca Raton, FL, 1991; pp 269–286.
35. Yu Z, Pancholi C, Bhagavathy GV, Kang HS, Nguyen JK and Ptaszek M. Strongly Conjugated Hydroporphyrin Dyads: Extensive Modification of Hydroporphyrins' Properties by Expanding the Conjugated System. *J. Org. Chem.* 2014; **79**: 7910–7925.
36. Kee HL, Nothdurft R, Muthiah C, Diers JR, Fan D, Ptaszek M, Bocian DF, Lindsey JD, Culver JP and Holten D. Examination of Chlorin-Bacteriochlorin Energy-Transfer Dyads as Prototypes for Near-infrared Molecular Imaging Probes. *Photochem. Photobiol.* 2008; **84**: 1061–1072.
37. Kee, HL, Diers JR, Ptaszek M, Muthiah C, Fan D, Lindsey JS, Bocian DF and Holten D. Chlorin-Bacteriochlorin Energy-transfer Dyads as Prototypes for Near-infrared Molecular Imaging Probes: Controlling Charge-transfer and Fluorescence Properties in Polar Media. *Photochem. Photobiol.* 2009; **85**: 909–920.
38. Kang HS, Esemoto NN, Diers JR, Niedzwiedzki DM, Greco JA, Akhigbe J, Yu Z, Pancholi C, Bhagavathy GV, Nguyen JK, Kirmaier C, Birge RR, Ptaszek M, Holten, D and Bocian DF. Effects of Strong Electronic Coupling in Chlorin and Bacteriochlorin Dyads. *J. Phys. Chem. A* 2016; **120**: 379–395.
39. Meares A, Bhagavathy GV, Zik SR and Gallagher T. Expanding p-Conjugation in Chlorins Using Ethenyl Linker. *J. Org. Chem.* 2018; **83**: 9076–9087.
40. Hu G, Liu R, Alexy EJ, Mandal AK, Bocian DF, Holten D and Lindsey JS. Panchromatic Chromophore-tetrapyrrole Light-harvesting Arrays Constructed from Bodipy, Perylene, Terrylene, Porphyrin, Chlorin, and Bacteriochlorin Building Blocks *New. J. Chem.* 2016; **40**: 8032–8052.
41. Diers JR, Tang Q, Hondros CJ, Chen CY, Holten D, Lindsey JS and Bocian D F. Vibronic Characteristics and Spin-Density Distributions in Bacteriochlorins as Revealed by Spectroscopic Studies of 16 Isotopologues. Implications for Energy- and Electron-Transfer in Natural Photosynthesis and Artificial Solar-Energy Conversion. *J. Phys. Chem. B.* 2014; **118**: 7520–7532.
42. Except for molecular mechanics and semi-empirical models, the calculation methods used in Spartan '10 have been documented in: Shao Y, Molnar LF, Jung Y, Kussmann J, Ochsenfeld C, Brown ST, Gilbert ATB, Slipchenko LV, Levchenko SV, O'Neill DP, DiStasio RA Jr, Lochan RC, Wang T, Beran GJO Besley NA, Herbert JM, Lin CY, Van Voorhis T, Chien SH, Sodt A, Steele RP, Rassolov VA, Maslen PE, Korambath PP, Adamson RD, Austin B, Baker J, Byrd EFC, Dachsel H, Doerksen RJ, Dreuw A, Dunietz BD, Dutoi AD, Furlani TR, Gwaltney SR, Heyden A, Hirata S, Hsu CP, Kedziora G, Khalliulin RZ, Klunzinger P, Lee AM, Lee MS, Liang WZ, Lotan I, Nair N, Peters B, Proynov EI, Pieniazek PA, Rhee YM, Ritchie J, Rosta E, Sherrill CD, Simmonett AC, Subotnik JE, Woodcock HL III, Zhang W, Bell AT, Chakraborty AK, Chipman DM, Keil FJ, Warshel A, Hehre WJ, Schaefer HF III, Kong J, Krylov AI, Gill PMW and Head-Gordon M. *Phys. Chem. Chem. Phys.* 2006; **8**: 3172–3191.
43. Ptaszek M, Lahaye D, Krayner M., Muthiah C and Lindsey JS. De Novo Synthesis of Long-Wavelength Absorbing Chlorin-13,15-dicarboximides. *J. Org. Chem.* 2010; **75**: 1659–1673.

44. Lamm JH, Glatthor J, Weddelling JH, Mix A, Chmiel J, Neumann B, Stammeler HG and Mitzel NW. Polyalkynylantracenes – Syntheses, Structures and their Behaviour towards UV Irradiation. *Org. Biomol. Chem.* 2014, **12**: 7355-7365.
45. Nierth A, Kobitski AY, Nienhaus U and Jäschke A. Anthracene-BODIPY Dyads as Fluorescent Sensors for Biocatalytic Diels-Alder Reactions. *J. Am. Chem. Soc.* 2010; **132**: 2646–2654.
46. Birks JB *Photophysics of Aromatic Molecules*, Wiley-Interscience, London, 1970; pp. 142–192.
47. Magdaong NCM, Taniguchi M, Diers JR, Niedzwiedzki DM, Kirmaier C, Lindsey JS, Bocian DF and Holten D. Photophysical Properties and Electronic Structure of Zinc(II) Porphyrins Bearing Zero to Four meso-Phenyl Substituents – Zinc Porphine to Zinc Tetraphenylporphyrin (ZnTPP). *J. Phys. Chem. A*. 2020; **124**: 7777–7794.
48. Felton RH. In *The Porphyrins*; Dolphin, D., Ed.; Academic Press: New York, 1978; Vol. V, pp. 53–126.
49. Shrestha K, González-Delgado JM, Blew JH and Jakubikova E. Electronic Structure of Covalently Linked Zinc Bacteriochlorin Molecular Arrays: Insights into Molecular Design for NIR Light Harvesting. *J. Phys. Chem. A* 2014; **118**: 9901–9913.
50. Bilsel O, Rodriguez J, Milam SN, Gorlin PA, Girolami GS, Suslick KS and Holten D. Electronic States and Optical Properties of Porphyrins in van der Waals Contact: Th^{IV} Sandwich Complexes. *J. Am. Chem. Soc.* 1992; **114**: 6528–6538.
51. Kasha M, Rawls HR and El-Bayoumi MA. The Exciton Model in Molecular Spectroscopy. *Pure Appl. Chem.* 1965; **11**: 371–392.
52. J. Wang, E.K. Yang, J. R. Diers, D. M. Niedzwiedzki, C. Kirmaier, D. F. Bocian, J. S. Lindsey, and Holten D. Distinct Photophysical and Electronic Characteristics of Strongly Coupled Dyads Containing a Perylene Accessory Pigment and a Porphyrin, Chlorin, or Bacteriochlorin. *J. Phys. Chem. B* 2013; **117**: 9288–9304.
53. Mandal AK, Diers JR, Niedzwiedzki DM, Hu G, Liu R, Alexy EJ, Lindsey JS, Bocian DF and Holten D. Tailoring Panchromatic Absorption and Excited-State Dynamics of Tetrapyrrole–Chromophore (Bodipy, Rylene) Arrays. The Interplay of Orbital Mixing and Configuration Interaction. *J. Am. Chem. Soc.* 2017; **139**: 17547–17564.
54. Yuen JM, Diers JR, Alexy EJ, Roy A, Mandal AK, Kang HS, Niedzwiedzki DM, Kirmaier C, Lindsey JS, Bocian DF and Holten D. Origin of Panchromaticity in Multichromophore–Tetrapyrrole Arrays. *J. Phys. Chem. A* 2018; **122**: 7181–7201.
55. Esemoto, NN, Satraitis A, Wiratan L and Ptaszek M. Symmetrical and Nonsymmetrical Meso–Meso Directly Linked Hydroporphyrin Dyads: Synthesis and Photochemical Properties. *Inorg. Chem.* 2018; **57**: 2977-2988.

Supplementary Information
for
Conjugated-Linker Dependence of the Photophysical Properties and
Electronic Structure of Chlorin Dyads

Hyun Suk Kang,[†] Andrius Satraitis,[‡] Adam Meares,[‡] Ganga Viswanathan Bhagavathy,[‡]
James R. Diers,[§] Dariusz M. Niedzwiedzki,[#] Christine Kirmaier,[†]
Marcin Ptaszek,^{*,‡} David F. Bocian,^{*,§} and Dewey Holten^{*,†}

[†]Department of Chemistry
Washington University
St. Louis, Missouri 63130-4889, United States

[‡]Department of Chemistry and Biochemistry
University of Maryland, Baltimore County
Baltimore, Maryland 21250, United States

[§]Department of Chemistry
University of California
Riverside, California 92521-0403, United States

[#]Center for Solar Energy and Energy Storage, and
Department of Energy, Environmental & Chemical Engineering
Washington University
St. Louis, MO 63130-4889
United States

Topic	Page
1. Syntheses of the Dyads	2
2. Absorption and Fluorescence Spectra of the Dyads and Benchmarks in Benzonitrile.....	4
3. Structure Characteristics of the Dyads.....	6

1. Synthesis of Dyads

General. ^1H NMR (400 or 500 MHz) and ^{13}C NMR (100 or 125 MHz) spectra were collected at room temperature in CDCl_3 unless noted otherwise. Chemical shifts (δ) were calibrated using solvent peaks (^1H signals: residual proton signals: 7.26 ppm for chloroform, ^{13}C signals: 77.16 for CDCl_3). Commercially available anhydrous toluene and DMF were used for palladium coupling reactions. All other solvents and commercially available reagents were used as received. FT-ICR analyzer was used for HRMS analyses.

Known compounds **Ch-EH**,³⁵ **Ch-Br**,⁴³ **Ch-EHm**,³⁹ **3**,⁴⁴ and **4**,⁴⁵ were prepared following the published procedures.

General procedure for palladium-catalyzed cross-coupling reaction. Samples of all solid reagents except palladium catalyst, and solvent were placed in the Schlenk flask and deoxygenated by freeze-thaw under nitrogen (3 cycle). Palladium catalyst was then added to the reaction flask and the reaction mixture was deoxygenated by freeze-thaw (1 cycle). Reaction flask was brought to the room temperature and placed in pre-heated oil bath and stirred as indicated below.

C2- β Bm. A mixture of **Ch-EHm** (9.7 mg, 0.020 mmol), $\text{Pd}_2(\text{dba})_3$ (2.8 mg, 0.0031 mmol) and $\text{P}(\text{o-tol})_3$ (3.7 mg, 0.012 mmol) in anhydrous toluene/triethylamine (5:1, 6 mL) were reacted at 60 °C. TLC after 1h showed the presence of starting material, hence $\text{Pd}_2(\text{dba})_3$ (2.8 mg, 0.0031 mmol) and $\text{P}(\text{o-tol})_3$ (3.7 mg, 0.012 mmol) were added and the reaction mixture was stirred at 60 °C for additional 2h, after which TLC showed the complete consumption of the starting material. The reaction mixture was concentrated and purified by column chromatography [silica, hexanes/ CH_2Cl_2 (2:1) \rightarrow neat CH_2Cl_2] afforded a brown solid (6 mg, 63%). ^1H NMR (CDCl_3): δ 9.71 (s, 2H), 9.37 (s, 2H), 9.19 (d, $J = 4.6$ Hz, 2H), 8.92 (d, $J = 4.6$ Hz, 2H), 8.86-8.84 (m, 6H), 8.48 (d, $J = 4.1$ Hz, 2H), 7.29 (s, 4H), 4.71 (s, 4H), 2.64 (s, 4H), 2.09 (s, 4H), 1.90 (s, 4H), -1.41 (bs, 2H), -1.79 (bs, 2H); ^{13}C NMR (CDCl_3): δ 176.8, 163.5, 152.8, 152.7, 142.1, 140.8, 139.2, 138.0, 137.4, 135.7, 133.0, 132.8, 132.1, 129.8, 129.1, 127.9, 124.5, 121.5, 115.1, 108.9, 106.8, 95.2, 94.7, 51.8, 46.8, 31.2, 29.8, 21.4; ESI-MS: $[\text{M}+1]^+$, $\text{M} = \text{C}_{66}\text{H}_{58}\text{N}_8$, Calcd: 963.4857, Obsd: 963.4890.

C2- β BD. Samples of **Ch-EHm** (14.3 mg, 0.029 mmol), 4,7-dibromobenzo[c]-1,2,5-thiadazole **1** (4.26 mg, 0.014 mmol), $\text{Pd}_2(\text{dba})_3$ (2.7 mg, 0.0029 mmol), and $\text{P}(\text{o-tol})_3$ (6.8 mg, 0.022 mmol) in toluene/ Et_3N (6 mL, 5:1) was stirred at 60 °C. Resulting mixture was washed with (water and brine), dried (Na_2SO_4), and concentrated to produce brown solid. Column chromatography [silica, hexane/dichloromethane (2:1)] yielded a red-brown solid (6.32 mg, 40%). ^1H NMR (CDCl_3 , 400 MHz) δ -1.80 (s, 2H), -1.41 (s, 2H), 1.91 (s, 12H), 2.11 (s, 12H), 2.64 (s, 6H), 4.77 (s, 4H), 7.28 (s, 4H), 8.20 (s, 2H), 8.49 (d, $J = 4.3$ Hz, 2H), 8.87 (d, $J = 4.3$ Hz, 2H), 8.86 (s, 2H), 8.91 (s, 2H), 8.93 (d, $J = 4.6$ Hz, 2H), 9.20 (d, $J = 4.6$ Hz, 2H), 9.55 (s, 2H), 9.72 (s, 2H). Due to the low solubility, ^{13}C NMR cannot be obtained. MS: $[\text{M}+\text{H}]^+$, $\text{M} = \text{C}_{72}\text{H}_{60}\text{N}_{10}\text{S}$: Calcd: 1097.479589, Obsd: (HRMS-ESI) 1097.477650.

C- β BD. A mixture of **Ch-EHm** (18 mg, 0.037 mmol), 4-bromobenzo[c][1,2,5]thiadiazole **2** (16 mg, 0.075 mmol) and $\text{PdCl}_2(\text{PPh}_3)_2$ (5.3 mg, 0.0076 mmol) in DMF/ NEt_3 (6 mL, 2:1) was stirred for 23 hours at 80 °C. The resulting mixture was washed (water and brine), dried (Na_2SO_4), and concentrated. Column chromatography [silica, hexane/dichloromethane (3:1) \rightarrow (2:1)] provided a brown-green solid (7.9 mg, 34%). ^1H NMR

(CDCl₃, 400 MHz) δ -1.86 (bs, 1H), -1.49 (bs, 1H), 1.89 (s, 6H), 2.08 (s, 6H), 2.63 (s, 3H), 4.72 (s, 2H), 7.27 (s, 2H), 7.72 (dd, $J_1 = 9.8$ Hz, $J_2 = 11.5$ Hz, 1H), 8.48 (d, $J = 4.3$ Hz, 1H), 8.89-8.84 (m, 3H), 8.92 (d, $J = 4.6$ Hz, 1H), 9.50 (s, 1H), 9.72 (s, 1H). ¹³C NMR (CDCl₃, 400 MHz) δ 21.5, 21.6, 31.2, 46.8, 51.9, 91.6, 92.2, 94.6, 95.3, 106.8, 117.7, 121.3, 122.0, 124.2, 127.9, 128.8, 129.0, 129.6, 131.8, 132.6, 133.0, 133.1, 135.4, 137.5, 137.9, 139.2, 140.1, 141.9, 152.4, 152.8, 154.9, 163.4, 176.5. MS: ([M+H]⁺, M = C₄₀H₃₄N₆S): Calcd: 617.2482, Obsd: (HRMS-ESI) 617.2494

C₂- β AC. A mixture of **Ch-Br** (20 mg, 0.037 mmol), 9,10-diethynylantracene **3** (4.2 mg, 0.018 mmol), Pd₂(dba)₃ (5.4 mg, 0.0044 mmol), and P(o-tol)₃ (13.5 mg, 0.044 mmol) in toluene/Et₃N mixture (6 mL, 5:1) was stirred for 12 hours at 60 °C. Resulting mixture was washed (water and brine), dried (Na₂SO₄), and concentrated to produce red-brown solid. Column chromatography [silica, hexane/CH₂Cl₂ (2:1)] yielded a red-brown solid (12.3 mg, 59%). ¹H NMR (CDCl₃, 400 MHz) δ -1.80 (s, 2H), -1.38 (s, 2H), 1.97 (s, 12H), 2.12 (s, 12H), 2.68 (s, 6H), 4.77 (s, 6H), 7.34 (s, 4H), 7.95 (m, 4H), 8.50 (d, $J = 4.2$ Hz, 2H), 8.89 (s, 2H), 8.89 (d, 4H), 8.94 (d, $J = 4.6$ Hz, 2H), 8.98 (s, 2H), 9.21 (d, $J = 4.6$ Hz, 2H), 9.29 (m, 4H), 9.61 (s, 2H), 9.76 (s, 2H); ¹³C NMR (CDCl₃, 400 MHz) δ 1.17, 14.3, 21.6, 21.7, 29.9, 31.3, 46.8, 52.1, 93.9, 94.7, 95.3, 98.2, 107.0, 117.2, 119.3, 121.1, 124.2, 127.4, 128.0, 129.0, 131.8, 132.7, 133.1, 133.4, 139.4, 140.1, 141.9, 152.3, 152.9, 163.4, 176.5; MS([M+H]⁺, M = C₈₀H₆₆N₈): Calcd: 1139.5483, Obsd: (HRMS-ESI) 1139.5438.

C- β AC. A mixture of **Ch-Br** (20 mg, 0.037 mmol), 9-ethynylantracene **4** (11.3 mg, 0.06 mmol), and PdCl₂(PPh₃)₂ (3.9 mg, 0.0056 mmol) in DMF/NEt₃ (6 mL, 2:1) was stirred for 2 hours at 80 °C. The resulting mixture was washed (water and brine), dried (Na₂SO₄), and concentrated to produce a dark brown-green solid. Column chromatography [silica, hexane/CH₂Cl₂ (3:1)] provided a brown solid (12 mg, 47%). ¹H NMR (CDCl₃, 400 MHz) δ -1.85 (bs, 1H), -1.47 (bs, 1H), 1.94 (s, 6H), 2.09 (s, 6H), 2.65 (s, 3H), 4.71 (s, 2H), 7.32 (s, 2H), 7.63 (t, $J = 7.0$ Hz, 2H), 7.79 (t, $J = 7.7$ Hz, 2H), 8.14 (d, $J = 8.4$ Hz, 2H), 8.49 (d, $J = 4.3$ Hz, 1H), 8.57 (s, 1H), 8.88 (m, 2H), 8.94 (d, $J = 4.7$ Hz, 2H), 9.13 (d, $J = 8.7$ Hz, 2H), 9.21 (d, $J = 4.6$ Hz, 1H), 9.57 (s, 1H), 9.76 (s, 1H); ¹³C NMR (CDCl₃, 400 MHz) δ 21.5, 21.6, 31.3, 46.8, 52.0, 93.5, 94.7, 95.3, 96.1, 107.0, 117.5, 117.8, 120.9, 124.0, 126.0, 127.1, 127.3, 128.0, 128.1, 128.8, 129.0, 131.6, 131.7, 133.1, 133.4, 135.2, 137.6, 137.9, 139.4, 140.1, 141.7, 152.1, 152.9, 163.4, 176.3; MS: ([M+H]⁺, M = C₄₇H₃₈N₄): Calcd: 659.3169, Obsd: (HRMS-ESI) 659.3145.

Dimethyl 2,2'-((2,5-dibromo-1,4-phenylene)bis(oxy)diacetate (5). A mixture of 2,5-dibromohydroquinone (0.881 g, 3.29 mmol) and K₂CO₃ (4.54 g, 32.9 mmol) in DMF (35 mL) was stirred under nitrogen at 60 °C for 30 min. A sample of methyl bromoacetate (1.56 mL, 16.4 mmol) was added and the resulting mixture was stirred at 60 °C for 1h. The mixture was allowed to cool to room temperature, filtered, and concentrated under high vacuum. The resulting pale brown solid was treated with a small amount of cold methanol and filtered to afford an off-white solid: (0.577 g, 61%). ¹H NMR (CDCl₃): δ 3.82 (s, 6H), 4.65 (s, 4H), 7.08 (s, 2H). The resulting product was used in the next step without further characterization.

C₂- β P. A mixture of **Ch-EH** (27.0 mg, 0.0594 mmol), **5** (11.1 mg, 0.0269 mmol), Pd₂(dba)₃ (8.2 mg, 0.0089 mmol), and P(o-tol)₃ (21.7 mg, 0.0713 mmol) in toluene/Et₃N (6 mL, 5:1) was reacted at 120 °C. for 5h. The reaction mixture was concentrated and purified by column chromatography [silica, hexanes/CH₂Cl₂ (1:1) \rightarrow neat CH₂Cl₂]. The resulting material was washed with MeOH, dried and chromatographed [silica, hexanes/CH₂Cl₂ (1:3)] to afford a

brown-green solid (8.6 mg, 25%). ¹HNMR (CDCl₃, 400 MHz) δ -1.96 (bs, 2H), -1.55 (bs, 2H), 2.10 (s, 12H), 2.50 (s, 6H), 3.93 (s, 6H), 4.75 (s, 4H), 5.10 (s, 4H), 7.46 (s, 2H), 7.58 (d, *J* = 7.8 Hz, 4H), 8.06 (d, *J* = 7.8 Hz, 4H), 8.06 (d, *J* = 4.4 Hz, 2H), 8.88 (s, 2H), 8.95-8.92 (m, two overlapped signals, 4H), 9.22 (d, *J* = 4.4 Hz, 2H), 9.49 (s, 2H), 9.78 (s, 2H). MS: ([M+H]⁺, M = C₇₄H₆₂N₈O₆): Calcd: 1159.4865, Obsd: (HRMS-ESI) 1159.4888.

2. Absorption and Fluorescence Spectra of Dyads and Benchmarks in Benzonitrile

Table S1. Spectral Characteristics of Chlorin Dyads and Benchmarks in Benzonitrile.

Compound	λ _B (nm)	λ _{Q2} (nm)	Δλ _{Q2} ^{shift} (cm ⁻¹)	λ _{Q1β} (nm)	λ _{Q1α} (nm)	Δλ _{Q1} ^{shift} (cm ⁻¹)	Δλ _{Q1} ^{split} (cm ⁻¹)	λ _{em} (nm)	fwhm em (nm)
<i>Current Dyads</i>									
C₂-βBm	407, 423, 453	539	244	673	683	471	218	686	16
C₂-βEm	404, 420, 450	540	278	668	689	479	456	693	15
C₂-βP	409, 421, 457	538	210	657 ^a	669	137	273	671	15
C₂-βAC	406, 418, 458 ^a	546	307	681	687 ^a	417	128	694	23
C₂-βBTD	404, 420, 446 ^a	546	342	663 ^a	682	210	420	689	26
C₂-βV	407, 421, 468	549	372	691 ^a	707	775	328	712	25
ZnC₂-βV	417	520	244	681 ^a	696		316	712	37
<i>Prior Dyads</i>									
C₂-βB	407, 424, 452	538	210	672	681	531	197	681	13
C₂-βE	405, 417, 452	538	174	664	687	436	504	687	13
<i>Current Benchmark Monomers</i>									
C-βEm	405, 420	532			657			658	15
C-βAC	421, 454	537			665			667	17
C-βBTD	407, 420, 462	536			662			665	18
C-βV	408, 422	538			663			665	17
<i>Prior Benchmark Monomers</i>									
C-βB	402, 418	532			653			652	13
C-βE	406, 420	533			656			656	13

^aShoulder on the main feature.

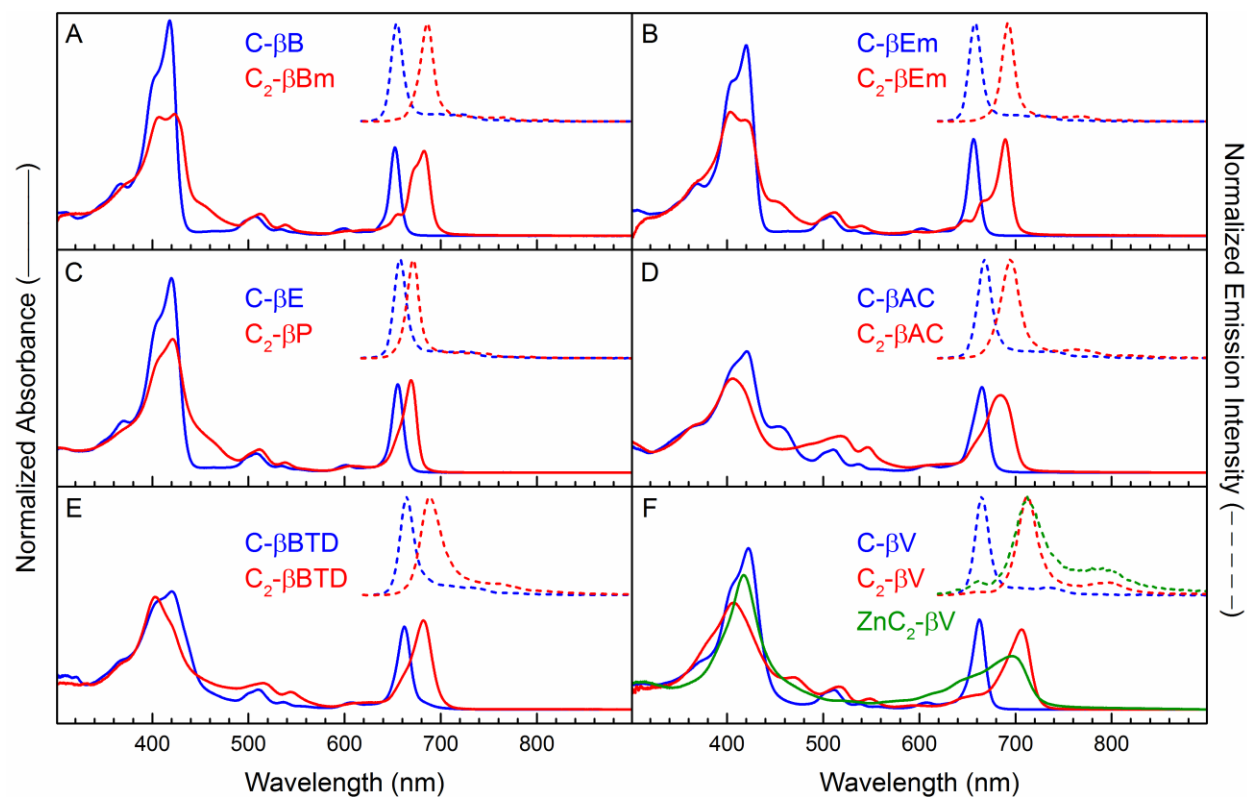


Figure S1. Absorption (solid) and fluorescence spectra (dashed) of the chlorin dyads (red) and benchmarks (blue) in benzonitrile. Absorption spectra were normalized to the total integrated intensity (300–1000 nm for spectra plotted vs cm^{-1}), and all fluorescence spectra (500–550 excitation) were normalized to the peak intensity.

3. Structure Characteristics of the Dyads

DFT calculations were performed on the dyads and benchmarks, starting with the optimized molecular geometry. The β -linked dyad **C₂- β Em**, like **C₂- β E** studied previously,²⁸ has a minimum energy structure with the bacteriochlorin macrocycles coplanar in an *anti*-conformation (Chart 2), for which the torsional angle (involving the bonds between the red atoms in Figure S2A) is defined as 180°. Accessing different torsional angles involves rotation about the linker axis. Regardless of the torsional angle for the minimum-energy structure, the barrier to internal rotation about the ethyne linker is quite low (<1.5 kcal/mol), consistent with previous calculations^{35,49} on the same or similar dyads.

The barrier to internal rotation is smaller (≤ 0.5 kcal/mol; Figure S2B) for dyad **C₂- β Bm**, like analog **C₂- β B** studied previously,³⁸ has minimum energy structure close ($\sim 10^\circ$) to the *syn*-coplanar conformation (defined as 0°). The calculation of the minimum energy for this dyad did not converge readily because there is little gradient toward the minimum. Thus, there is uncertainty in the global and local minima, compounding the low barriers that allow the dyad to sample essentially the full space of internal rotational conformations at room temperature ($k_B T \sim 0.6$ kcal/mol).

Probing the torsional potential for dyads **C₂- β V**, **C₂- β P**, **C₂- β AC** and **C₂- β BTd** involved stepping the dihedral angle involving the bonds between the atoms shown in red in Figure S2C-F between $\sim 0^\circ$ and $\sim 180^\circ$ and allowing the program to adjust the dihedral angle involving bond between the atoms shown in blue to seek the energy minimum. The latter variable angle (involving blue-labeled atoms) generally assumed a narrow range for the calculations for which the results are shown in Figures S2C-F with approximate limits as follows: **C₂- β V** (161° – 179°), **C₂- β P** (156° – 164°), **C₂- β AC** (1° – 30°), and **C₂- β BTd** (1° – 8°). The calculation results given in

Figure S2 indicate that **C₂-βV** and **C₂-βP** have a minimum near the *anti*-conformation (180°) while **C₂-βAC** and **C₂-βBTD** have a minimum near the *syn*-conformation (0°). The torsional barrier is low for **C₂-βAC** (<1.5 kcal/mol) and progressively increases for **C₂-βBTD** (~3 kcal/mole), **C₂-βP** (~4 kcal/mole) and **C₂-βV** (~ 5 kcal/mol) (Figure S2). One must view these barriers with caution. Only one trajectory on the multi-dimensional surface guided by one set of constraints and free (fit) angles for each of these dyads was explored. There are many sets of constrained or fit parameters that one could employ to further map the torsional potential. Such calculations could reveal lower barriers than those depicted in Figures S2C–F.

A relatively high torsional barrier associated with rotation about the vinyl linker for **C₂-βV** (Figure S2C) seems plausible given that motions removing two chlorins from an approximate coplanar arrangement effectively reduces conjugation involving the vinyl group. Given the low barrier calculated for butadiyne-linked dyad **C₂-βm** (Figure S2B), one might have expected a reasonably low barrier for dyads **C₂-βP**, **C₂-βAC** and **C₂-βBTD** given the longer distance between chlorins via the incorporation of an aromatic ring between the two ethynes (Figures S2D–F). Perhaps steric interactions involving the alkoxy-like substituents on the central phenyl ring of **C₂-βP** are involved, at least for the trajectory employed for Figure S2F. The angle between phenyl and the chlorins in the optimized geometry is (~15°). The structures **C₂-βAC** and **C₂-βBTD** were explored further as described below.

Figure S3 gives four potential conformations of **C₂-βAC** for which the overall energy and MO properties are calculated using DFT (Table S2). Several observations are noteworthy. (1) The *syn*-conformation (structure 2) has slightly (by 0.1-0.2 kcal/mol) lower energy than the *anti*-conformation (structure 1). (2) For either the *anti*-or *syn*-conformation, the anthracene is twisted about 20–22° from the plane(s) of the chlorins. (3) Structure 3, in which anthracene is twisted

90° from both chlorin macrocycles has highest energy of the four conformations explored, and this energy is ~5 kJ/mol higher than that of the minimized form. For this conformation, the two chlorins are substantially decoupled, as evidence by the pairs of degenerate, or nearly degenerate MOs, rather than pairs of split MOs as discussed below (e.g., HOMO and HOMO-1 both -4.93 eV; HOMO-2 and HOMO-3 both at -5.10 eV; Table S2). (4) The conformation in which one chlorin and the anthracene are coplanar and the second chlorin rotated 90° (structure 4) still supports some electronic coupling between the macrocycles as evidenced by the energy splittings between pairs of interacting MOs (e.g., -4.79 and -4.92 for the HOMO and HOMO-1 pair).

Figure S3 shows three potential conformations of **C₂-βBTD** for which the overall energy and MO properties are shown in the last three columns of Table S2. The lowest energy of the three conformations is structure 3, for which annotations are given at the lower right of Figure S2. This structure has the *syn*-conformation in which the benzotriazole (BTD) ring is flipped so that there is a short (3.14 Å) distance, and potential hydrogen-bonding (or other non-covalent) interaction, between a BTD nitrogen atom and the nearby hydrogen atom at the 15-position of the adjacent chlorin. Such interactions in structure 3 may underlie in part the significant stabilization (~8/3 kJ/mol) compared to the *syn*-conformation in which the BTD ring is flipped 180° (structure 2). The *anti*-conformation has an intermediate energy (structure 1). The optimized structure for structure 3 suggest that potential BTD-chlorin interactions may also give rise to a slightly bent bonds between the chlorins and the BTD. Such an effect is not observed for the structure 2, in which the flipped BTD ring removes the potential interactions between the BTD nitrogens and the chlorin 15-hydrogens that could pull the entities closer together. Such interactions in structure 3 could also contribute to the larger barrier for rotation of the chlorins with respect to the linker for there is a large rotation barrier for **C₂-βBTD** compared to **C₂-βAC**

(Figures S2E versus S2D). A more rigid structure for **C₂-βBTD** versus **C₂-βAC** could also contribute to the overall narrower long-wavelength (C₁ or Q_y-like) absorption manifold of the former compared to the latter (Figure 1E versus 1D).

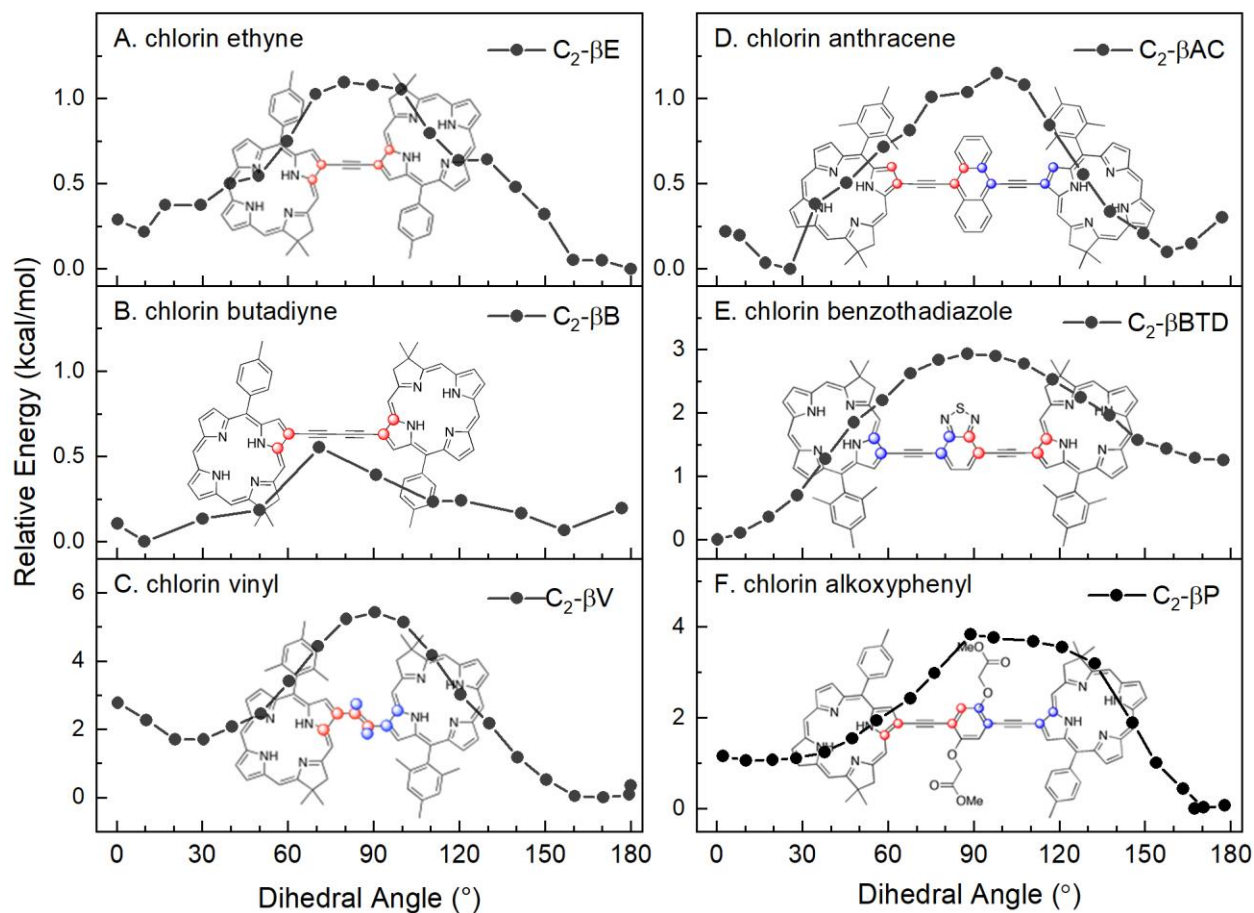


Figure S2. Relative total energy versus dihedral angle for chlorin dyads.

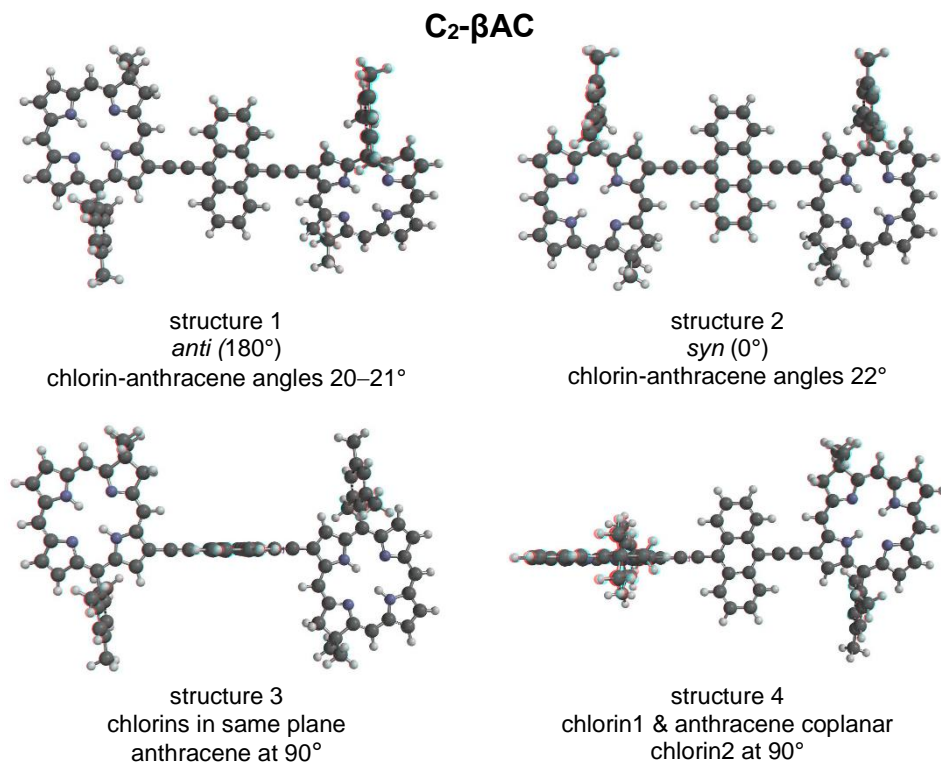


Figure S3. Four different potential conformations (structures) of dyad C₂-βAC for which the calculated overall energy and MO characteristics are shown in Table 5.

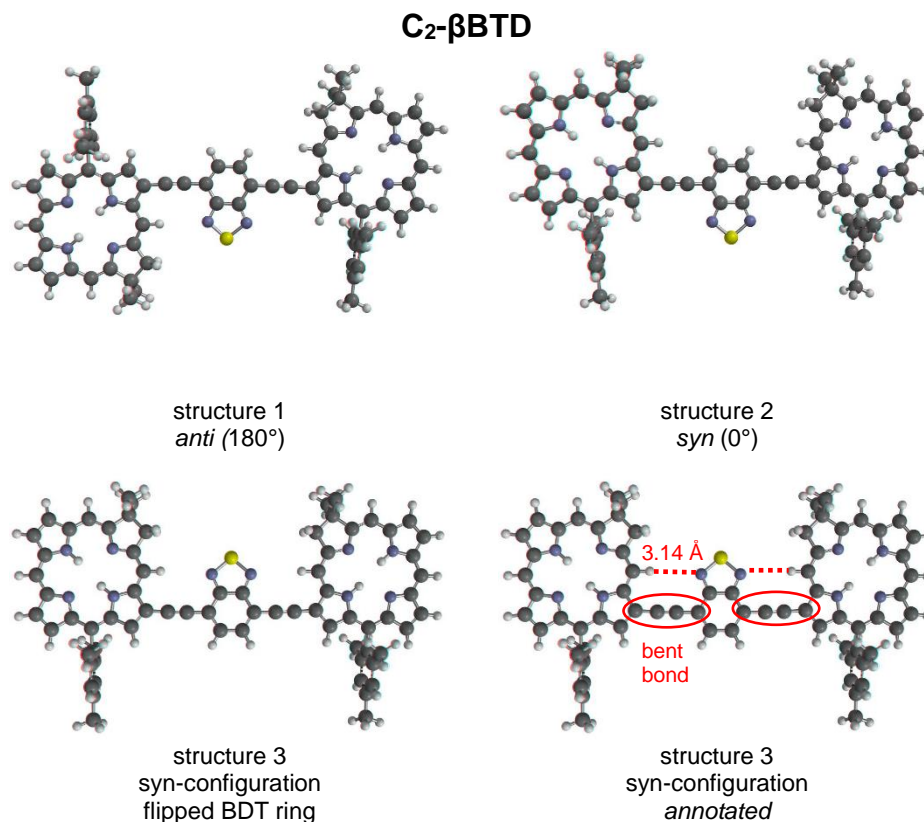


Figure S4. Three different potential conformations (structures) of dyad **C₂-βBTD** for which the calculated overall energy and MO characteristics are shown in Table 5. Structure 3 at the lower right is annotated to indicate a bent bond and a potential hydrogen-bonding interaction.

Table S2 Energy-minimized structural and MO information for dyads **C2-βAC** and **C2-βBTD**.^a

Structure	C ₂ -βAC				C ₂ -βBTD		
	1	2	3	4	1	2	3
E (kJ/mol)	-9258207	-9258207	-9258198	-9258202	-9781171	-9781168	-9781176
ΔE (kJ/mol)	0.54	0	8.89	4.99	4.54	8.35	0
LUMO+3 (eV)	-1.77	-1.76	-1.76	-1.78	-1.80	-1.79	-1.76
LUMO+2 (eV)	-1.94	-1.93	-2.13	-2.00	-2.19	-2.18	-2.21
LUMO+1 (eV)	-2.32	-2.31	-2.33	-2.33	-2.33	-2.34	-2.31
LUMO (eV)	-2.58	-2.55	-2.34	-2.50	-2.77	-2.75	-2.79
HOMO (eV)	-4.67	-4.66	-4.93	-4.79	-4.80	-4.82	-4.79
HOMO-1 (eV)	-4.99	-4.97	-4.93	-4.92	-5.00	-5.02	-4.99
HOMO-2 (eV)	-5.10	-5.06	-5.10	-5.09	-5.08	-5.13	-5.10
HOMO-3 (eV)	-5.13	-5.08	-5.10	-5.11	-5.15	-5.15	-5.11

^aSee structures in Figures 4 and 5. ΔE is the energy of the structure relative to that of the structure chosen as a reference for which ΔE = 0). The electron density in some of the MOs is localized primarily in the linker (see text).

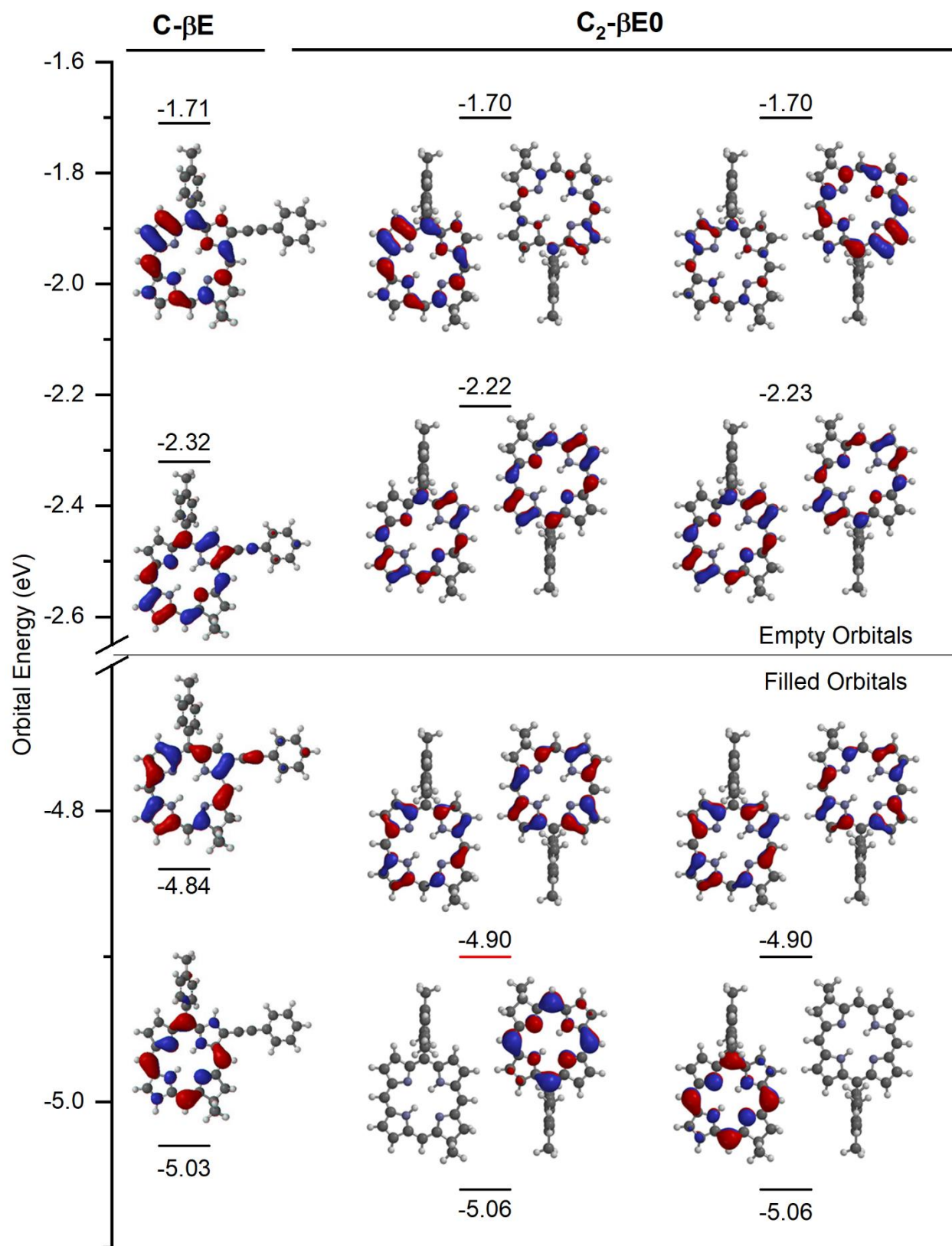


Figure S5. Frontier MOs and energies of benchmark chlorin **C-βE** and dyad **C₂-βE0** in which the linker was removed with the structure frozen at the optimized geometry for dyad **C₂-βE** (Chart 1).

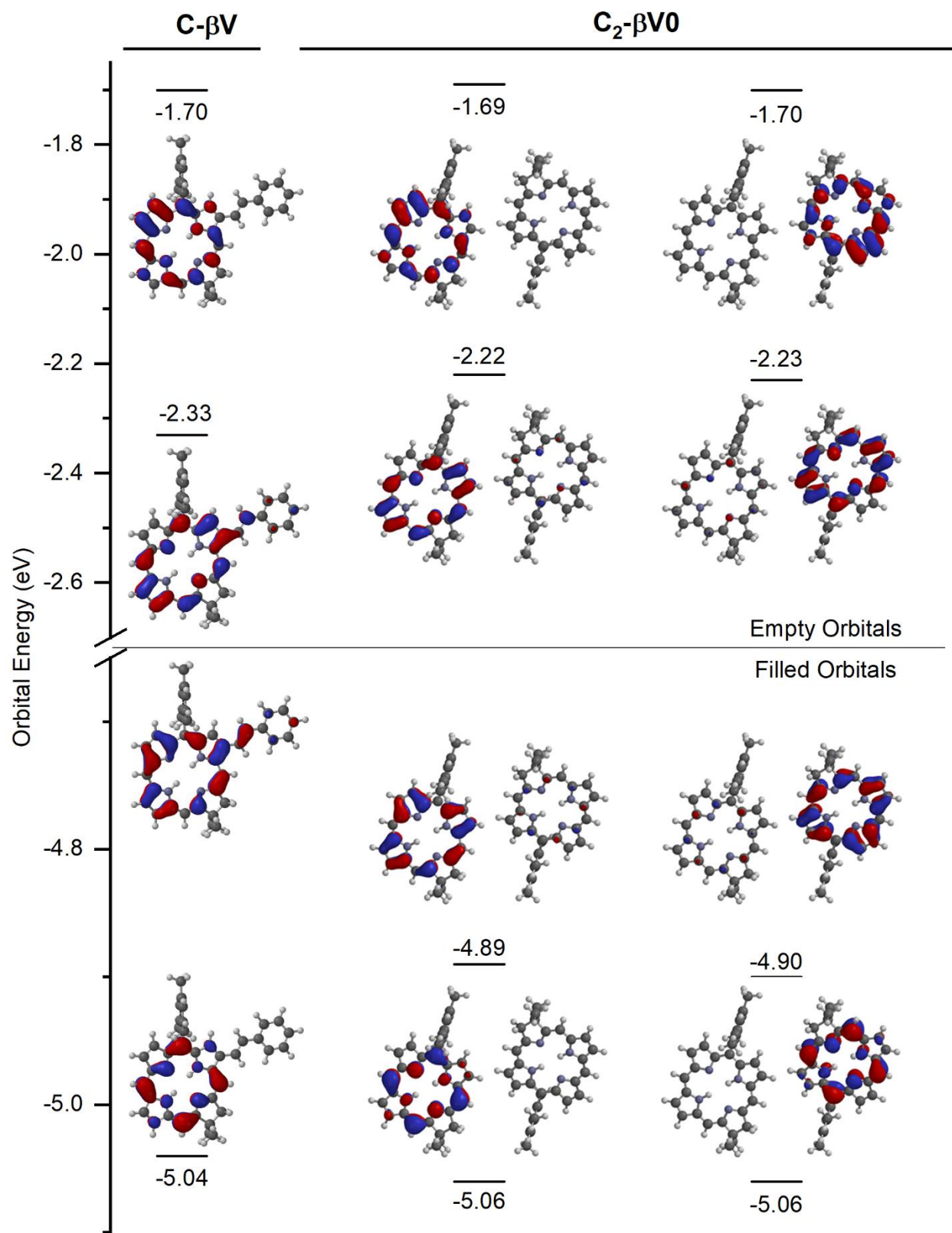


Figure S6. Frontier MOs and energies of benchmark chlorin **C-βV** and dyad **C₂-βV0** in which the linker was removed with the structure frozen at the optimized geometry for dyad **C₂-βV** (Chart 2).

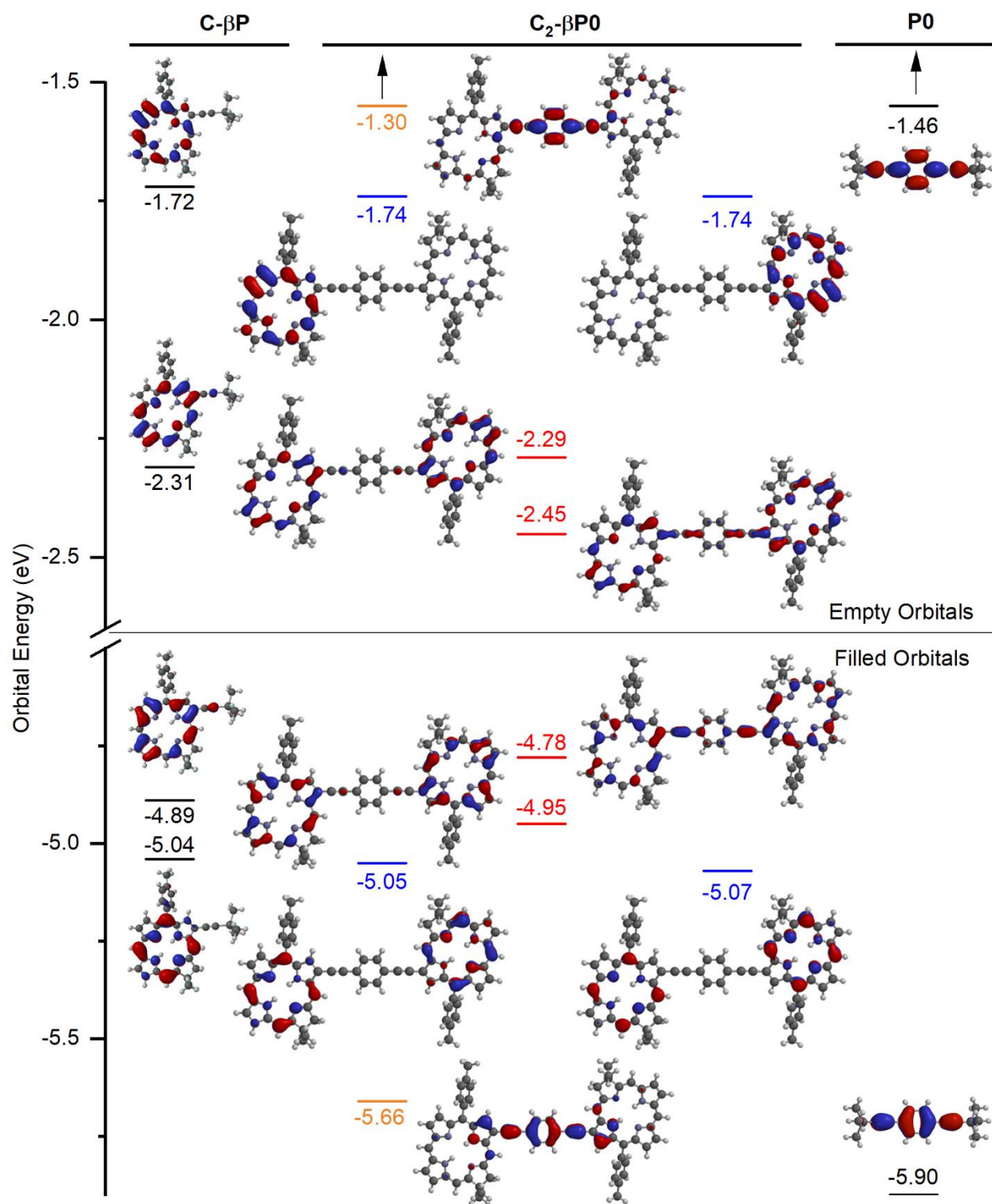


Figure S7. Frontier MOs and energies of fictive dyad **C₂-βP0**, benchmark chlorin **C-βP**, and benchmark **P0** linker. The color-coding is as in Figure 3. This dyad and the linker lack the alkoxy-like substituents on the phenyl ring of the linker that are present in **C₂-βP** (see Chart 2 and Figure 6).